Russian Chemical Reviews **73** (12) 1211 – 1238 (2004) © 2004 Russian Academy of Sciences and Turpion Ltd

DOI 10.1070/RC2004v073n12ABEH000833

Methodological, applied and thermodynamic aspects of hydrogen sorption by graphite and related carbon nanostructures

Yu S Nechaev, O K Alekseeva

Contents

I.	Introduction	1211
II.	Experimental studies of hydrogen sorption by carbon nanostructures	1212
III.	Theoretical studies of physisorption and chemisorption	1220
IV.	A thermodynamic analysis of the experimental data	1224
V.	Conclusion	1235

Abstract. Results of the experimental and theoretical investigations into hydrogen sorption by various carbon nanostructures, including fullerenes, single-walled and multi-walled nanotubes, nanofibres, nanographite and nanographite-based composites are surveyed. Results of a thermodynamic analysis of the most significant experimental data are presented. The emphasis is placed on the studies reporting the extremum sorption parameters. The thermodynamic and kinetic (diffusion) parameters and equations describing the sorption processes are refined. The prospects of the applications of new carbon nanomaterials for hydrogen storage in the automotive industry are discussed. The bibliography includes 206 references.

I. Introduction

Hydrogen represents a unique energy-rich fuel and highly efficient energy carrier.[1] The modern trends in the development of large-scale production of energy carriers and the automotive industry imply gradual replacement of non-renewable hydrocarbon fuels with hydrogen as an environmentally friendly processing product of water and biomass (which are renewable natural resources). This may only be achieved if either the problem of hydrogen storage and transportation † is successfully solved or autonomous systems for its *in situ* production are designed.

The governments of several countries have approved federal programmes aimed at the development of hydrogen-driven mobile motor vehicles. In the U.S., president Bush's initiative[2] has given a high priority to this programme. At the end of November 2003, the International Partnership for the Hydrogen Economy (IPHE) was founded, which joined 15 countries, including Russia. One of the major goals declared by the IPHE is the design of competitive affordable electric vehicles operated with hydrogen fuel cells by 2020. In December 2003, the Complex program of R&D activities in the field of hydrogen energetics and fuel cells was approved in Russia.[3] A prerequisite for all these programmes is the development of compact systems of hydrogen storage that would provide sufficiently fast desorption of hydrogen in a technically reasonable temperature range.[2,4–8]

According to the basic qualifying standards of the U.S. Department of Energy (DOE), the prospective stand-alone systems should store no less than 6.5 mass % or 62 kg m^{-3} of hydrogen (to guarantee a haul of $\sim$500 km) ‡ and operate with in the technologically acceptable temperature and time regimes to be commercially justified.§

The potential utility of carbon-based light sorbents for hydrogen storage was pointed out as early as in the 1960s. The best performance for cryoadsorption storage has been achieved for adsorbents based on low-density high-surface-area activated carbons, which also enabled purification of molecular hydrogen from admixtures. In particular, porous carbon AX-21, which is characterised by a specific surface area of 3000 m^2 g^{-1}, adsorbs up to 10 mass % (or 32 kg m^{-3}) of hydrogen at 77 K and 5 MPa (50 atm). However, the adsorption capacity of this material as well as of other activated carbons drops down to 0.5 mass % at room temperature and 7 MPa,[9,10] which is hardly acceptable for the automotive industry.

The interest of researchers in the hydrogen sorption by carbon materials has been rekindled following the discovery of new allotropic forms of carbon, *viz*., fullerenes, nanotubes, graphite nanofibres and other nanostructured carbon materials.[11–13] These carbon materials are composed of quasi-sp^2-hybridised carbon atoms assembled into closed spherical (fullerenes), non-spherical clusters or quasi-one-dimensional tubes seamlessly rolled-up from graphene sheets. Nanotubes are subdivided into single-walled (with a diameter of 1 – 2 nm) and multi-walled (with a diameter of 10 – 40 nm) species.[12,14–17] The latter may contain from 2 to 50 graphene layers. Graphite nanofibres are built up of graphite platelets stacked at different angles with respect to the

Yu S Nechaev G V Kurdjumov Institute of Metals Science and Physics, State Research Centre of the Russian Federation, I P Bardin Central Research Institute of Ferrous Metallurgy, 2-ya Baumanskaya ul. 9/23, 105005 Moscow, Russian Federation. Fax (7-095) 777 93 50. E-mail: nechaev@online.ru
O K Alekseeva Institute of Hydrogen Energy and Plasma Technology, Russian Research Centre 'Kurchatov Institute', pl. Kurchatova 1, 123182 Moscow, Russian Federation. Fax (7-095) 196 62 78. Tel. (7-095) 196 73 90. E-mail: alex@hepti.kiae.ru

Received 14 July 2003
Uspekhi Khimii **73** (12) 1308 – 1337 (2004); translated by Ya V Zubavichus

† According to estimates,[1] the long-distance transportation of hydrogen through the pipe lines at a pressure of 7 – 8 MPa (70 – 80 atm) is less expensive than the electric power transmission through the high-voltage lines.

‡ A typical motor vehicle requires $\sim$0.04 m^3 of a hydrocarbon fuel to travel 500 km, whereas an electric vehicle driven by a hydrogen fuel cell requires 2 – 4 kg of H_2 for the same haul.[4–6]

§ Networked or autonomous hydrogen storage systems should conform to common qualifying standards: ignition time $\sim$15 s, refueling time $<$ 5 min, working lifetime (no less than 500 cycles) at a fuel regeneration level no lower than 90%.

fibre axis (*i.e.*, parallel, perpendicular or in a herringbone arrangement). Typically, the fibres possess lengths of 5 – 100 μm and diameters of 1 – 500 nm.

The first experimental results reporting increased hydrogen sorption (5 mass % – 10 mass % under normal conditions) by a material consisting of single-walled carbon nanotubes were published in 1997.[18] Numerous investigations into hydrogen sorption by various carbon nanomaterials and their metal-doped modifications that followed have demonstrated that the required sorption capacity at room temperature and a reasonable pressure is difficult to achieve but is attainable, in principle.[4, 18 – 26] For instance, nanographite adsorbs hydrogen sufficiently well but its applications are hampered by typically high desorption temperatures.[22, 27 – 31] Furthermore, it turned out that the sorption capacities could be different by as much as two – three orders of magnitude even for closely related materials. In 1998, exceptionally high hydrogen sorption (up to 67 mass %) by graphite nanofibres (GNF) at room temperature and 12 MPa was reported.[32, 33] These communications evoked both great interest and many critical comments.[34 – 37]

Several factors can be responsible for the observed scatter in the experimental hydrogen sorption capacities by different carbon nanomaterials. The major reasons for the discrepancies in quantitative estimates of sorption properties of carbon nanomaterials include difficulties in the preparation of pure sorbents with a strictly defined microstructure, the lack of commonly adopted techniques for their attestation, complexity of physical and chemical processes in their interactions with hydrogen and dependence of these processes on the experimental conditions.[14, 34, 38 – 40] These, as well as a number of other aspects of the interactions of carbon sorbents with hydrogen, became a subject of vivid discussion at conferences during 2001 – 2004.[41 – 51] The same issues were analysed in a number of reviews devoted to fullerenes,[52] fullerites,[52, 53] carbon nanotubes, graphite nanofibres[14, 52, 54 – 57] and other carbon nanostructures[4, 14, 22, 58 – 62] (see also http://asyncbrain.baf.cz/sanatorium/1/h2fuel/).

Although some sceptics have pointed out that 'reliable data on carbon nanostructures are lacking and the experimental results are characterised by poor reproducibility', many researchers (for instance, see Refs 10, 14, 42 – 47, 51, 63 – 65) share the opinion that all aspects of the problem deserve a more accurate and thorough consideration and soundly propose to continue investigations within the scope of an international project 'Physicochemical fundamentals and prospects in the use of new carbon materials for hydrogen storage in automotive industry'.[48] The present review describes for the first time an original constructive analysis of thermodynamic and diffusion parameters as applied to a series of hydrogen – carbon sorbent systems that are characterised by the extremum characteristics of the sorption processes.

II. Experimental studies of hydrogen sorption by carbon nanostructures

Table 1 summarises experimental data on sorption (and storage) of hydrogen by various carbon nanomaterials (CNM), such as fullerenes, single- and multi-walled nanotubes (SWNT and MWNT, respectively), carbon and graphite nanofibres (CNF and GNF, respectively), nanographite and composites on its base and new types of nanostructures, such as fullerene-filled nanotubes ('peas in the pod'), nanobells, *etc*. Micrographs of some of these nanostructures are shown in Fig. 1. An analysis of the factors influencing the results of sorption capacity determination indicates that even carbon materials belonging to one type differ strongly from each other. For example, nanotubes synthesised using different methods can differ in purity, diameter, length, specific surface area, *etc*. The apparent sorption capacity of such materials is also strongly affected by the character of the chemical or thermal pretreatment of the samples and purity of hydrogen.[106]

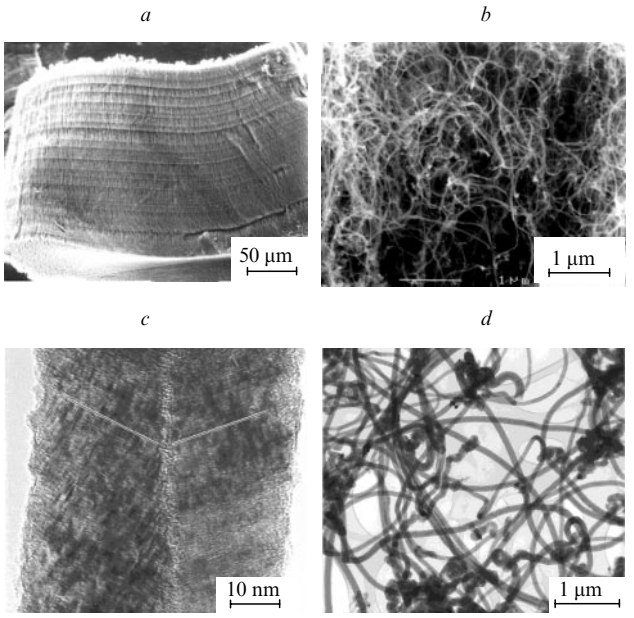


Figure 1. Micrographs of some carbon nanostructures.[32, 91] (*a*) A dense block of aligned (straightened) carbon nanotubes prepared by catalytic pyrolysis of ferrocene on a quartz support, (*b*) randomly oriented carbon nanotubes, (*c*) GNF composed of graphite platelets oriented at 45° (herringbone-type) with respect to the fibre axis, (*d*) GNF prepared by catalytic decomposition of an ethylene – hydrogen mixture.

Quantitative estimates of the sorption capacities discussed in the present review are based on several experimental techniques, such as volumetric analysis (VA), thermogravimetric analysis (TGA), temperature-programmed desorption (TPD) and thermodesorption spectroscopy (TDS). The apparent values of the sorption capacity of carbon nanomaterials can differ from the real ones if possible sources of the experimental errors are neglected.¶

In particular, in the case of volumetric analysis (*i.e.*, when a change in the volume or pressure of hydrogen due to sorption or desorption is measured), the following factors should be taken into account:

— temperature effects (that are especially significant for high-pressure experiments),

— thermal effects due to compression/decompression of the sorbent upon sorption/desorption of hydrogen,

— thermal effects due to nuclear spin transitions (changes in the ratio of ortho/para modifications of molecular hydrogen),

— the actual equilibration time,

— possible leaks in the experimental setup (which can strongly decrease the accuracy of determination of small changes in pressure).

Tibbetts *et al.*[38] studied sorption of hydrogen at 300 K and 10 MPa and estimated that a decrease in the temperature by 1° for a sample with a mass of 1 g in a volume of 1 litre necessitates that the pressure was increased by 33.3 kPa, which results in an apparent increase in the amount of absorbed hydrogen by 2.6 mass %. They found that filling of the chamber with hydrogen was accompanied by a jump-like increase in temperature by more than 25 °C and the system required about 100 min to equilibrate.

TGA and TDS data can become less accurate due to admixtures of water vapour and other gases in hydrogen (*e.g.*, sample No. 26 in Table 1).[39, 40] The experimental errors are often aggravated by insufficient purity of sorbents themselves (in particular, due to admixtures of catalysts).

¶ For a discussion concerning potential sources of the experimental errors, see, for instance, Refs 1, 34, 38, 56.

Table 1. Results of experimental studies of hydrogen sorption by carbon nanomaterials.

No	Sorbent and its characteristics	Sample mass /mg	Sorbent preparation method	Sorbent pretreatment method	T /K [a]	P /MPa	H_2 (mass %) (sorption)	Measurement method [b] (hydrogen purity)	Comments	Ref.
Porous carbon										
1	AX-21, $S_{sp} = 3000\ m^2\ g^{-1}$				77 300	5 7	10 0.5			9
	AX-21, $S_{sp} = 2000\ m^2\ g^{-1}$				77	3.5	5.3			66
2	Saran, $S_{sp} = 1600\ m^2\ g^{-1}$		pyrolysis of poly(vinylidene chloride)		77 300	0.3 16	2.4 0.4	VM		35
3	Nanoporous carbon (total porosity ~70%), mean pore size ~0.8 nm, $S_{sp} = 1200\ m^2\ g^{-1}$				520–970	20	1.3	TPD, MS, electroresistance	sorption and desorption kinetics were studied	67
4	Pyrolytic graphite				323–363	30–50	~0.1	TPD		68, 69
Carbon nanotubes										
5	SWNT, diameter of 1.3 nm (contains 90% of amorphous carbon)		electric arc	milling in a ball mill for 24 h in Ar	RT	0.08	<0.1	TPD		34
6	SWNT ropes, diameter of 13 nm, $S_{sp} = 285\ m^2\ g^{-1}$	200	laser ablation	sonication	80	12	8.25	VM (H_2 99.9999%)	the isotherms pressure *vs.* composition were measured	70
7	SWNT, diameter of 1.85 nm	500	electric arc (hydrogen)	no treatment	RT	12–10	2.4	VM (H_2 99.999%)		71
				chemical treatment	RT	12–10	2.8			
				chemical treatment and annealing in vacuum	RT	12–10	4.2 [c]			
8	SWNT	160–350	catalytic decomposition of acetylene	heating in NaOH acidic treatment	RT RT	10 10	5.15 2.67	hydrogen adsorption	effects of surface treatment were observed	23
9	SWNT, $S_{sp} = 263\ m^2\ g^{-1}$	10	DEL (Dynamic Enterprises Limited)	cold compacting with Au powder	293		0.9	ECM		72
				cold compacting	78	0.2	0.6	TPD		72
10	SWNT (long bundles), diameter of 1.69 nm	500	catalytic decomposition of hydrocarbons	no treatment chemical treatment chemical treatment and annealing in vacuum	RT RT RT	11 11 11	2.4 2.8 4.2	VM		24

Table 1 (continued).

No	Sorbent and its characteristics	Sample mass /mg	Sorbent preparation method	Sorbent pretreatment method	T /K [a]	P /MPa	H_2 (mass %) (sorption)	Measurement method [b] (hydrogen purity)	Comments	Ref.
Carbon nanotubes										
11	SWNT		laser ablation	sonication, purification	RT	0.1	7	TPD, VM		4, 25, 73
12	SWNT in the form of peapods, bundles (C_{60}@SWNT)		Nd : YAG, laser ablation, Ni/Co catalyst	chemical and thermal purification	RT	6		TPD	a peak of H_2 desorption is observed at 350 K	74
				additional treatment with NaOH	RT	6				
13	SWNT in the form of peapods, bundles (C_{60}@SWNT)		the same	chemical treatment with NaOH	RT	6		TPD	adsorption of molecular hydrogen at 365 K	75
14	SWNT ropes, bundles (mats), diameter of tubes 1.4 nm, diameter of bundles 15 nm		electric arc (Carbolex, Inc.)	no treatment	500	0.1		thermo-EMF		76
				the same	77	0.2 – 0.3	1.2	TGA, thermo-EMF, electroresistance (H_2 99.999%)		76
				oxidation and chemical treatment with						
				4.0 M HCl	77	0.2 – 0.3	3.5			
				HNO_3	77	0.2 – 0.3	6.5			
15	Purified SWNT (purity of 90 mass % – 95 mass %), diameter of 1.38 nm	1000	laser ablation, Ni/Co catalyst	chemical and thermal treatment	295	9	0.32	TPD	activation energy of desorption was estimated (E_d = 9.6 kJ mol^{-1})	77
16	CNT									
	aligned bundles, S_{sp} = 61 m^2 g^{-1}		catalytic pyrolysis	no treatment	RT	10	3.5	VM (H_2 > 99.999%)	a new compact structure was formed under the action of hydrogen	78
	random ordered bundles		the same	the same	RT	10	0.5			
17	CNT ('amorphous', diameter of 10 – 60 nm)	200	floating catalyst method	no treatment	RT	10	1.3	VM (H_2 99.999%)	adsorption during 24 h; structure of the samples was similar to GNF (herringbone-type)	79
				annealing at						
				1700 °C			1.6			
				1900 °C			2.2			
				2000 °C			2.3			
				2200 °C			4.0			
18	SWNT, bundles	500	laser ablation, Ni/Co catalyst	no treatment	200		0.05	inelastic neutron scattering	hydrogen storage below 200 K does not require external pressure; hydrogen desorbs at T > 200 K	80
				chemical treatment	200		1.2			
19	SWNT		electric arc, Co/Ni, YNi_2 catalysts	purification	123	2.5	2.4	VM, TPD (H_2 99.9999%)	H_2 desorbs at 723 K (0.24% of H_2 adsorbs reversibly)	81

Table 1 (continued).

No	Sorbent and its characteristics	Sample mass /mg	Sorbent preparation method	Sorbent pretreatment method	T /K [a]	P /MPa	H_2 (mass %) (sorption)	Measurement method [b] (hydrogen purity)	Comments	Ref.
Carbon nanotubes										
20	SWNT	1000	HiPco, Carbon Nanotechnologies, Inc.	thermal treatment	RT	8	0.43	VM		82
21	SWNT, aligned long ropes	500 – 800	electric arc	cold pressed into pellets (without binder)	295	11	4.0 [d]	VM	70% of H_2 desorbs upon release of high pressure; the sample meets the requirements for automotive industry	83
22	SWNT	30 – 50	Tubes@Rice	no treatment	RT	4.8	0.4	microbalance	chemical treatment increases the sorption by a factor of 3	84
				mild oxidation in CO_2 and thermal treatment	RT	4.8	1.2			
23	SWNT, diameter of 1.3 nm				295	0.1	0.94			85
					77	0.1	2.37			
24	CNT, diameter of 20 – 30 nm	200	pyrolysis of acetylene, catalysts:					VM		86
			AB_5 hydrides	no treatment	298	10	2.4			
				purification	298	10	3.3			
			AB_2 hydrides	no treatment	298	10	2.3			86
				purification	298	10	3.1			
25	CNT doped with transition metals				RT		0.5 – 1.0	TGA	preliminary results	87
26	K-MWNT, S_{sp} = 148 $m^2\ g^{-1}$	10	catalytic decomposition of methane	chemical and thermal treatment in He	293 – 373	0.1	1.8 [e]	TGA, TPD (H_2 99.999%)		39
							12			
	Li-MWNT, S_{sp} = 148 $m^2\ g^{-1}$	10	the same	the same	293 – 373	0.1	2.5 [e]			
							21			
27	MWNT (aligned, cone-shaped), diameter of 50 – 100 nm	1	CVD [f]	no treatment	RT	0.2	0	TPD (H_2 99.999%)		88
				the same	RT	1	5 – 7			
				thermal treatment	RT	0.2	7.8			
				thermal and chemical treatment	RT	1	8.8 – 13.8 [g]			
28	MWNT in the form of curls, S_{sp} = 263 $m^2\ g^{-1}$, internal diameter of 5 – 15 nm, external diameter of 10 – 30 nm	2	CVD [f]	no treatment	300	4	0.67	TPD (H_2 99.999%)		89
	Aligned MWNT, S_{sp} = 877 $m^2\ g^{-1}$, internal diameter of 8 nm, external diameter of 20 nm	2	CVD [f]	the same	300	4	1.97	TPD (H_2 99.999%)		89

Table 1 (continued).

No	Sorbent and its characteristics	Sample mass /mg	Sorbent preparation method	Sorbent pretreatment method	T /K [a]	P /MPa	H_2 (mass %) (sorption)	Measurement method [b] (hydrogen purity)	Comments	Ref.
Carbon nanotubes										
29	MWNT samples with cracks in external walls	100	catalytic synthesis	no treatment	RT	10	1.3	VM	hydrogen sorption	90
				annealing	RT	10	4.0	(H_2 99.999%)	during 24 h	
	MWNT samples without cracks	100	the same	no treatment	RT	10	0.73			
				annealing	RT	10	0.81			
30	Highly-oriented closed MWNT, diameter of 10 – 40 nm, S_{sp} = 60 m^2 g^{-1}	100	catalytic pyrolysis	heeting to 373 K, 24 h	290	10	2.4	VM	adsorption of H_2 results in formation of microchannels	91
	randomly oriented closed MWNT, S_{sp} = 27 m^2 g^{-1}	100	the same		290	10	0.68			
31	MWNT, open	200 – 500	template synthesis	thermal and chemical treatment, annealing in vacuum	77	10	6.46	VM	sorption of H_2 in subnanopores	92
					RT	10	1.12	(H_2 99.999%)		
Carbon and graphite nanofibres										
32	GNF, tubular structure	21.4	catalytic decomposition of hydrocarbons	chemical treatment for removal of metal particles of the catalyst	RT	12	11.26	VM		33
	GNF, herringbone structure	318.8	the same	the same	RT	12	57.85			
		291.4	"	"	RT	12	67.55 [h]			
		103.7	"	"	RT	12	60.58			
	GNF, platelet structure	103.2	"	"	RT	12	53.68			
		101.4	"	"	RT	12	43.63			
33	GNF	> 1000	catalytic decomposition of hydrocarbons	annealing in vacuum (423 K, 5 h)	RT	12	40	VM	reversible changes in the crystal lattice parameters are possible (d increases from 0.340 nm to 0.347 nm)	93
34	GNF	500 – 1000	catalytic decomposition of a $C_2H_4 - CO - H_2$ mixture	annealing in an inert atmosphere *in situ*	RT	12	40	VM, TGA, TPD, XRD		32
	GNF	500 – 1000	the same	no treatment	RT	12	2			
35	GNF, S_{sp} = 25 m^2 g^{-1}	300	catalytic decomposition of ethylene	annealing in vacuum at 1173 K	77	0.45	0.17	VM		35
					300	16	0.25			
	GNF, S_{sp} = 23 m^2 g^{-1}	300	the same	the same	77	0.45	–			
					300	16	0.2			

Table 1 (continued).

No	Sorbent and its characteristics	Sample mass /mg	Sorbent preparation method	Sorbent pretreatment method	T /K [a]	P /MPa	H_2 (mass %) (sorption)	Measurement method [b] (hydrogen purity)	Comments	Ref.
Carbon and graphite nanofibres										
36	CNF, $S_{sp} = 300\ m^2\ g^{-1}$ CNF, $S_{sp} = 2290\ m^2\ g^{-1}$		commercial product the same	without activation activation	300 300	6 6	0.1 0.6	VM		94
37	GNF	1750	catalytic decomposition of ethylene	annealing in vacuum at 423 K activation	290 290	12 12	10 15	VM, XRD	the $P-C-T$ phase diagram was determined, several sorption – desorption cycles were completed	95 – 97
38	GNF		pyrolysis	no treatment pretreatment	RT RT	12 12	4.18 6.54			20
39	CNF, herringbone structure, diameter of 200 – 500 nm	10 – 20	catalytic decomposition of ethylene	no treatment doping with KNO_3	303 303	0.1 0.1	0.34 4.9	TGA/QMS, XRD (H_2 99.999%)	doping with KNO_3 increases concentration of H_2 by < 0.3 mass %	98
40	CNF	300 – 1000	catalytic pyrolysis	thermal treatment in Ar thermal treatment in vacuum washing with deionised water	RT RT RT	11 11 11	3.4 4.5 5.7	VM	$LaNi_5$ was used as a standard	24
41	Activated CNF		commercial samples	–	77	2	2.8	VM	reversible physisorption in subnanopores	99
42	CNF, herringbone structure	500	catalytic decomposition of CH_4, catalyst Ni – MgO	thermal treatment in N_2 at 1473 K	298	12	1.4	VM (H_2 99.999%)		36
Miscellaneous carbon nanomaterials										
43	SWNH, nanohorns, $S_{sp} = 1006\ m^2\ g^{-1}$ (SWNH content 95%)		laser ablation	oxidation at 693 K	77 77 196 303	0.1 2 – 3 6.5 6.5	0.5 2.5 0.95 0.3	gravimetry (a balance with a precision within 0.1 μg)		100
44	Multi-walled nanobarrels	471.7	reaction of Al_4C_3 with halogens (gas)		77 300	10 10	6.2 3.2	(H_2 99.999%)		101
45	C-N-Nanobells (oriented), diameter of 15 nm, length of 50 nm		CVD [f]	treatment with N_2 plasma + chemical treatment	RT	1	8	QMS, TGA (H_2 99.999%)	ten cycles were completed	21
46	Nanographite, $S_{sp} = 10\ m^2\ g^{-1}$		mechanochemical synthesis in a ball mill at $P_{H_2} \approx 1$ MPa and 300 K		373	1	7.4	TPD, NMR, neutron diffraction	hydrogen desorbs at an elevated temperature	27 – 31

Table 1 (continued).

No	Sorbent and its characteristics	Sample mass /mg	Sorbent preparation method	Sorbent pretreatment method	T /K [a]	P /MPa	H_2 (mass %) (sorption)	Measurement method [b] (hydrogen purity)	Comments	Ref.
Miscellaneous carbon nanomaterials										
47	Nanographite, $S_{sp} = 780\ m^2\ g^{-1}$	1000	mechanochemical synthesis in a ball mill in vacuum	thermal treatment	RT	6.0	0.20 – 0.25	VM (H_2 99.99999%)	five sorption – desorption cycles were completed (formation of pores with $d < 1.0$ nm was observed)	102
	Initial graphite, $S_{sp} = 7\ m^2\ g^{-1}$	1000	the same	the same	RT	6.0	0.02			
48	Nitrogen-doped nanographite		CVD [f]	plasma treatment	RT	7	0.7 – 0.8	TGA		64
49	Fullerites C_{60}, C_{60}/C_{70}			liquid phase hydrogenation	453	2.4 – 2.8	6	pressure change		103
50	Fullerites C_{60}				723 – 773	3000 – 7000	5.0 – 7.9			19
51	Films of nanostructured carbon, $S_{sp} = 665\ m^2\ g^{-1}$	1.25	ultrasound-assisted cluster deposition	annealing in an Ar flow (150 °C, 1 h)	RT	0.1	1.1	TPD , NEXAFS		104, 105

[a] RT is room temperature. [b] Adopted acronyms: VM is volumometry, TPD is temperature-programmed desorption, MS is mass spectrometry, ECM is electrochemical methods, TGA is thermogravimetric analysis, XRD is X-ray diffraction, QMS is quadrupole mass spectrometry, NEXAFS is Near-edge X-ray absorption fine structure. [c] Total amount of desorbed H_2 is 4.2 mass % (3.3 mass % at RT and 0.9 mass % upon heating). [d] Volume capacity is 68 kg m^{-3}. [e] Corrected data from Ref. 40, which reported overestimated values due to utilisation of humid hydrogen for similar samples. [f] CVD stands for chemical vapour deposition. [g] Desorption of hydrogen occurs upon heating to 573 K. [h] Total amount of desorbed H_2 is 45.09 mass %.

As can be seen from Table 1, DOE requirements to the parameters of hydrogen sorption by carbon nanostructures have been met in several cases (*e.g.*, sample Nos 11, 27, 32–34, 37, Table 1). In particular, hydrogen sorption capacity at room temperature and 12 MPa (measured using a Sieverts-type apparatus) has reached ~67 mass % (!) for specific GNF samples prepared by metal-catalysed (typically, Ni, Fe) pyrolysis of hydrocarbons at 723–1023 K (sample No. 32).[33] These fibres were composed of graphite platelets with lengths of 10–100 μm and thicknesses of 3–50 nm oriented parallel (tubular-type fibres), perpendicular (platelet-type fibres) and at an acute angle (herringbone-type fibres) with respect to the fibre axis; the minimum distance between the platelets was 0.335 nm. The authors of this study suggested [33] that the structures of these materials are ideally suited for hydrogen storage. Desorption occurred within 5–10 min. Later, the same authors in response to criticism from other researchers, noted [32] that a special thermal pretreatment of the fibres aimed at the removal of chemisorbed gases and water is necessary to provide reproducible results. Sorption capacity of the samples increased from 2 mass % to 40 mass % (sample No. 34, Table 1) as a result of an *in situ* thermal treatment in an inert gas.[32]

Attempts undertaken by several other research groups to reproduce these results failed despite the experimental conditions being strictly observed.[35, 36, 94, 107] Nevertheless, attainability of high sorption capacities for similar structures has been confirmed in other studies [20, 24, 95–97] (sample Nos 37, 38, 40, Table 1).

Recently, a continuous process for the synthesis of MWNT using hot-filament plasma-assisted chemical vapour deposition has been developed.[88] The structure of MWNT prepared using this method (sample No. 27, Table 1) differs from the ideal one and resembles to a certain extent that of the graphite nanofibres having graphite platelets with open ends. These materials are characterised by relatively high and reproducible sorption capacity (5 mass % – 7 mass %) at room temperature and moderate pressures (1 MPa). Annealing of the samples at 573 K and removal of admixtures of catalysts gave rise to an increase in the sorption capacity up to 13.8 mass %.

Note that volume density of hydrogen is also of importance for applications: it should be no less than 62 kg m^{-3}. According to estimates,[5] volume density of hydrogen sorbed by an array of nanotubes with a diameter of 2 nm can reach 54 kg m^{-3} assuming that density of the original nanotubes is ~1000 kg m^{-3}. Indeed, density of the standard carbon adsorbents lies in the range of 500–1000 kg m^{-3}, but that of CNT is typically significantly lower, *viz.*, 100–200 kg m^{-3}. Only pressed bundles of nanotubes had a density of ~330 kg m^{-3}, which corresponded to the volume density of absorbed hydrogen of 10–33 kg m^{-3} at a sorption capacity of 10 mass %. Recently developed methods for the compaction of CNT enable preparation of materials with a density of as high as ~800 kg m^{-3} (see Ref. 56) and even 1700 kg m^{-3} (see Ref. 83). In the latter case, promising results with respect to hydrogen sorption have been obtained: the volume density of hydrogen reached 68 kg m^{-3} at a sorption capacity of 4 mass % (sample No. 21, Table 1).

Not all the experimental results look so promising (see, for instance, data for sample Nos 5, 15, 20, 35, 36, Table 1). According to measurements [38] performed in a temperature and pressure range of 193–773 K and 3.5–11 MPa for nine samples including graphite flakes, activated carbon G-60 with a specific surface area of 700 m^2 g^{-1}, carbon wires (grown on a FeNiCu composite), graphitised carbon fibres, PYROGRAF fibres and MWNT with different diameters, the hydrogen sorption capacity at room temperature did not exceed 0.1 mass % at 3.5 MPa and 0.5 mass % at 11 MPa. All attempts to activate the samples did not give positive results. A study of hydrogen sorption by purified SWNT samples as well as by differently pretreated samples of SWNT, MWNT and GNF prepared using the CVD method [37] has given similar results: the maximum hydrogen uptake did not exceed 0.63 mass % at room temperature and 4.5 MPa.

One possible route to enhance sorption capacity of carbon nanomaterials is development of alternative synthetic approaches. A series of experimental studies (see, for instance, reviews [108, 109]) has shown that a high sorption capacity can be achieved by implantation of atoms or ions of hydrogen isotopes with a kinetic energy on the order of 10 keV into graphite or by sputtering of graphite (or another graphite material) with a hydrogen plasma. In the latter case, amorphous 'a-C : H' films are deposited onto metallic walls of the plasmatron. Such films are characterised by a high tritium content (T/C ≈ 0.5–0.7), which corresponds to a sorption capacity of 4.2 mass % – 5.8 mass % (recalculated for the same protium content).

The prospects of the application of less typical forms of nanostructured carbon as hydrogen sorbents were recently discussed by Rawat *et al.*[110] They synthesised liquid crystals of carbon doped with carbon nanofibres and found that sorption of hydrogen by the material increased linearly in a pressure range of 0.3–0.6 MPa (at 77 K) and reached 3.5 mass % at 0.6 MPa (that is the maximum pressure achievable with their experimental setup); extrapolation of the experimental results to a pressure of 2.5 MPa gave a sorption capacity of 6.5 mass %. A new class of 'pillared' materials based on nanographite and nanotubes doped with lithium was proposed [111] as potential hydrogen sorbents. These materials are characterised by an increased separation between layers of graphite or walls of nanotubes, which can enhance their sorption capacity. Unfortunately, for the moment, these materials exist only in theory although the authors proposed possible routes to their synthesis. According to estimates,[111] the hydrogen sorption capacity of these materials at room temperature and 2–5 MPa can reach as high as 6.0 mass % – 6.5 mass % (or 61.7–62.9 kg m^{-3}), depending on the exact structure.

Investigations into the electrochemical accumulation of hydrogen in carbon nanomaterials are also of great interest.[65, 72, 112–121] In the majority of cases, the measurements were conducted in a system of half-cells filled with 6–7 M KOH (as an electrolyte) at room temperature with the working electrode made of the respective metallised carbon nanomaterial. In this case, the charge/discharge processes, which occur on the working electrode, can be represented as:

$$\mathrm{CNM} + x\,\mathrm{H_2O} + \mathrm{e^-} \underset{\text{discharge}}{\overset{\text{charge}}{\rightleftharpoons}} (\mathrm{CNM} + x\,\mathrm{H}) + x\,\mathrm{OH^-}\,.$$

A series of carbon materials including various CNT, SWNT and MWNT have been studied with respect to the electrochemical accumulation of hydrogen.[112] In this case, the hydrogen sorption capacity can reach 2.0 mass % at 298 K, partly due to metallic admixtures. For an SWNT sample, a discharge capacity of 316 mA h g^{-1} was achieved,[112] which corresponds to a hydrogen sorption capacity of 1.2 mass %. The capacity was virtually independent of the number of charge–discharge cycles. The most significant experimental and theoretical studies on the electrochemical sorption of hydrogen by carbon nanotubes (CNT) have been recently surveyed.[113] Good results were obtained for the CNF decorated with Ni–P alloy particles.[114] A high discharge capacity of 1625 mA h g^{-1} (which corresponds to a hydrogen sorption capacity of 5.7 mass %) was also obtained for the electrodes prepared by compacting a mixture of CNT, copper powder and polymer binder (polytetrafluoroethylene, or PTFE) taken in a mass proportion 1 : 5 : 3 into a nickel collector.[116] No doubt, the electrochemical accumulation of hydrogen in systems with carbon electrodes will find applications in the future,[65, 72] although development of the electrodes on the basis of less expensive activated carbons seems more promising due to a high cost of CNT.[119]

Different physical methods, such as NMR (see Refs 122–125), neutron scattering,[80, 126–135] ESR,[136] Raman scattering, are normally applied to elucidate the mechanisms of hydrogen accumulation in the storage systems under development.[137] In particular, it has been demonstrated that physisorption of hydro-

gen molecules by SWNT bundles at 200 K occurred predominantly in the internal channel-cavities,[128] although sorption centres were observed on the external surfaces of SWNT as well.[129] The ^{1}H NMR data [125] supported the presence of sorption centres both on the external surfaces of SWNT and in the internal channels (the authors observed mutual diffusion of hydrogen molecules between the two types of the centres). An analysis of the ESR spectra indicates that hydrogen adsorbs dominantly on admixtures since the signal caused by admixtures attenuates upon hydrogen adsorption. In the case of an MWNT sample synthesised without metal catalysts, the experimental data were interpreted as evidence for the direct interaction of hydrogen with the walls of the tubes.[136] An analysis of the Raman scattering spectra for an H_2–MWNT system has revealed an influence of the method used for the synthesis of the MWNT on the hydrogen uptake and confirmed that hydrogen can be adsorbed not only in the molecular form but in the dissociated atomic form as well.[137]

III. Theoretical studies of physisorption and chemisorption

The great interest to the problems of hydrogen storage has promoted numerous theoretical investigtions into the interactions of molecular and atomic hydrogen with carbon nanostructures. This interest was to a large extent stimulated by impressive results obtained in the field of spherical carbon clusters and nanosized tubes [12, 15, 16] as well as by the relative simplicity of the species being adsorbed and availability of efficient computational methods (advantages and disadvantages of the modern computational approaches have been analysed elsewhere [138, 139]). Table 2 summarises the theoretical results obtained using different models, which are of greatest importance for the following discussion. Supplementary information may be found elsewhere,[4, 14, 56, 57, 61] in particular, in two recent reviews (Refs 138, 152).

All theoretical studies can be formally subdivided into two main groups. The first group of studies analyses idealised models of physisorption of molecular hydrogen whereas the second group elucidates the mechanisms of chemisorption of molecular and atomic hydrogen.

1. Physisorption of molecular hydrogen by carbon nanomaterials

The Monte Carlo method, classical molecular mechanics algorithms and approved sets of empirical potentials were applied to simulate physisorption of hydrogen by carbon nanostructures.[57, 94, 140, 142, 144, 153–155] Additionally, some of the simulations explicitly took into account the quantum effects.[139, 141, 144, 155] Virtually in all simulations, calculated sorption capacities of isolated ideal single-walled nanotubes with cylindrical pores as well as of graphite nanofibers with slot-like pores agree with the experimental data at 77 K but do not support the possibility of detection of a high sorption capacity at 300 K (see Table 2).

Figure 2 depicts schematically different areas of a bundle of SWNT available to adsorption of molecular hydrogen.[155, 156]

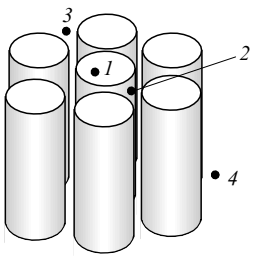


Figure 2. Sorption of hydrogen by an SWNT bundle.[155, 156]
(*1*) Inside the nanotube, (*2*) in the channels between the nanotubes, (*3*) in a 'groove', (*4*) on the outer surface of the bundle.

According to calculations of sorption of molecular hydrogen within the density functional theory (DFT), the inner space of the nanotubes, their outer surfaces and channels between them can be involved in the sorption process.[157] Adsorption in channels and slots is favoured over the adsorption on individual nanotubes.[156] An explicit account for the curvature of the surface of SWNT (which is of especially great importance for nanotubes with small diameters) indicates [158] that adsorption on the internal surface of the tube is energetically less favourable than that on the external surface. The probability of adsorption in extremely narrow channels between the tubes is also quite low (sample No. 9, Table 2).[135]

An increase in the sorption capacity can be achieved by optimising the size of the nanotubes and their arrangement within bundles.[140, 144, 145] Two typical types of arrangement of CNT in a bundle are shown in Fig. 3 [142] (samples No. 3, 9, 10, 11, Table 2). Probably, the arrangement of CNT giving rise to bundles with a triangular cross-section can ensure fairly high sorption levels even at room temperature provided that some specific conditions are met (sample No. 11, Table 2).[145] Changes in the parameters of the lattice formed by parallel bundles of single- or multi-walled nanotubes due to hydrogen sorption have been analysed by Cabli *et al.*[159, 160] and Gordilio *et al.*[161] Sorption capacity of SWNT bundles at 298 K and 12 MPa can be enhanced by 40% by doping them with alkali metals (sample No. 12, Table 2).[57]

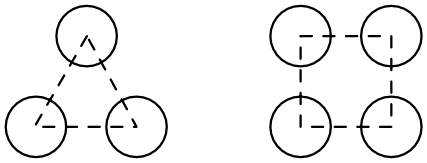


Figure 3. Bundles of CNT with triangular and square cross-sections.[142]

The results of simulations of molecular hydrogen sorption inside SWNT in a wide temperature (20–300 K) and pressure (up to 20 MPa) ranges [139] are of special note. An analysis of the computational data obtained within the density functional theory showed that changes in the external pressure can induce a series of first-order phase tranitions accompanied by abrupt changes in the density of adsorbed hydrogen. According to estimates,[139] the amount of adsorbed hydrogen at 290 K and 10 MPa does not exceed 0.42 mass % (sample No. 6, Table 2). A simulation of the interactions in the system H_2–SWNT using molecular dynamics methods and density functional theory has confirmed that molecular hydrogen adsorbed inside SWNT can undergo condensation to form quasi-one-dimensional crystal lattices at low temperature or one-dimensional associates with a variable density at high temperature.[162]

Recently, the effects exerted by a surface chemical modification of SWNT on hydrogen physisorption have been elucidated [143] (sample No. 8, Table 2). According to simulations based on a combination of the Monte Carlo and molecular dynamics methods, oxidation (which opens holes in the walls of the nanotubes) increases the sorption capacity whereas the presence of the surface C–H groups results in its decrease.

In summary, the above investigations clearly indicate that physisorption alone cannot be responsible for the high values of sorption capacities at high temperatures observed experimentally.

2. Interaction of atomic hydrogen with carbon nanostructures

There are a number of experimental facts that imply that the interaction of hydrogen with graphite and related carbon nanostructures cannot be reduced to a mere physisorption of molecular hydrogen and a more complex process has to be considered. These include an unexpectedly low rate of sorption, stepwise desorption occurring with an increase in temperature and evident effects of

Table 2. Selected theoretical estimates of parameters of hydrogen sorption on carbon nanomaterials.

No	Sorbent	Sorbent's basic parameters [a]	T /K	P /MPa	H_2 (mass %)	H_2 /kg m^{-3}	Computational methods [b] (comments)	Ref.
Physisorption								
1	Nanotubes	d = 2 nm			5.1		simple geometrical estimate	4
2	Nanotubes	d /nm					GCMC, Lennard-Jones potential	94
		0.7	300	10	0.8	10		
		0.7	300	30	0.5	14		
		1.0	300	10	0.6	9		
		1.0	300	30	1.1	15		
	Slitpores	h /nm						
		0.7	300	6	0.7			
		0.7	300	10	1.1			
		1.0	300	30	1.8			
		1.0	300	30	2.5			
3	Nanotubes (open), in a densely packed BTCS [c] configuration	d = 1.33 nm, $l \approx 0.6$ nm	298	1	0.15	1.45	the same	140
			298	10	1.0	10.4		
			298	20	1.6	16.5		
4	SWNT	d /nm					GCMC, Silvera – Goldman potential for the H – H and Crowell – Brown potential for the H – C interactions	141
	isolated	2.4	77	10	15.5	–		
		2.4	77	4	11	–		
		1.2	77	10	15	40		
		1.2	77	4	10	35		
	arrays	2.4	77	10	4.5	8		
		2.4	77	4	3.6	4		
		2.4	298	10	0.85	6		
		2.4	298	4	0.4	3		
		1.2	298	10	0.4			
		1.2	298	4	0.2			
	Slitpores	h /nm						
		0.6	98	10	0.2			
		0.9	298	10	0.45			
		1.2	298	10	0.40			
		2.0	298	10	0.36			
5	SWNT	d /nm					DFT (data on overall H_2 sorption inside and outside the nanotubes are given)	142
	isolated	1.225	77	4	8.1			
		2.04	77	4	9.5			
		2.719	77	4	9.6			
		a mixture	300	16	< 1			
	arrays	1.225	77	4.2	4.2			
		2.04	77	3.8	6.3			
		2.719	77	4	7.1			
		a mixture	300	16	< 1			
6	SWNT (isolated)	d = 0.4 nm	290	10	0.42		DFT	139
7	SWNT	S_{sp} /m^2 g^{-1}					GCMC, Silvera – Goldman potential for the H – H interactions and Lennard-Jones potential for the C – H_2 interactions (S_{sp} values were calculated)	115
	isolated (10.10)	2676	77	10	9.6			
		2676	300	10	1.3			
	bundles of 3 parallel tubes	2070	77	10	7.0			
		2070	300	10	1			
	bundles of 19 parallel tubes	1333	77	10	4.3			
		1333	300	10	0.6			
8	Defectless SWNT						GCMC, MD (effects of a surface chemical modification were estimated)	143
	(15,0) SWNT		77	20	6.8	60		
			77	40	7.1	62		
			293	20	2	15		
			293	40	3.1	25		
	(15,0) SWNT containing 10% of surface C – H groups		77	20	6.5	57		
			77	40	6.9	60		
			293	20	1.9	14		
			293	40	3	24		

Table 2 (continued).

No	Sorbent	Sorbent's basic parameters [a]	T /K	P /MPa	H_2 (mass %)	H_2 /kg m^{-3}	Computational methods [b] (comments)	Ref.
Physisorption								
8	Defectless SWNT						GCMC, MD (effects of a surface chemical modification were estimated)	143
	(6,6) SWNT		77	20	6.0	55		
			77	40	6.5	57		
			293	20	1.8	15		
			293	40	2.6	22		
	(6,6) SWNT after oxidation of 40% of the surface		77	20	8.0	60		
			77	40	8.6	65		
			293	20	2.0	15		
			293	40	3.4	23		
9	SWNT in a densely packed BTCS [c] configuration	d = 1.35 nm, $l \approx$ 0.21 nm	77	1	0.54		DFT	135
			300	53	0.54			
10	SWNT in a densely packed BSCS [d] configuration	d = 2.2 nm, $l \approx$ 1.1 nm	77	10	11.24	60	GCMC, Lennard-Jones potentials	144
11	SWNT (open), arrays in a BTCS [c] configuration	d = 0.6 nm, $l \approx$ 3 nm	77	7	33		the same	145
		d = 6 nm, $l \approx$ 1 nm	298	10	4.7			
	Slitpores	h = 0.6 nm	77	7	4.2 – 15.3			
			298	7	0.5 – 1.9			
12	SWNT (bundles) doped with alkali metals		298	12	2		GCMC, Silvera – Goldman potential for the H – H interactions and Lennard-Jones potential for the C – H_2 interactions	57
	dopant-free		298	12	1.4			
Chemisorption								
13	(5,5), (9,0) and (10,0) CNT (closed)				8		DFT/MM (in a stable configuration with 50% of H atoms inside and 50% thereof outside the tubes)	146
14	Isolated (10,10) SWNT				14	160	DFT with periodic boundary conditions	147
	MWNT				7.7			
15	(5,5) SWNT (capsule)				3.5	142	MD, Tersoff – Brenner and Lennard-Jones potentials; a selected part [atomic H (16 – 25 eV) inside the SWNT] *ab initio*	148 – 150
	(9,0) SWNT (capsule)				5.0	172		
	(10,10) SWNT (capsule)				9.1	177		
16	Carbon nanostructures				7.7		DFT (the maximum possible value for chemisorption, contribution of physisorption is insignificant)	151

[a] Notations used: d is a diameter of the nanotube, h is a pore size, l is the minimum distance between walls of the nanotubes. [b] Acronyms used: GCMC is Grand Canonical Monte Carlo, DFT is Density Functional Theory, MD is Molecular Dynamics, MM is Molecular Mechanics. [c] BTCS is bundles with a triangular cross-section. [d] BSCS is bundles with a square cross-section.

catalysts (for instance, Fe, Co or Ni), structural defects and other factors favouring dissociation of hydrogen molecules.[163, 164]

The use of the *ab initio* methods to study chemisorption is quite difficult due to the fact that a correct representation of the carbon nanostructure (*e.g.*, SWNT) requires a model containing approximately 200 atoms.[138] There are two principal ways to overcome this difficulty. The first one is based on the periodicity of the structure of SWNT, which makes it possible to adapt *ab initio* and DFT methods suitable for small systems to larger extended structures using periodic boundary conditions.[147, 165] The second way exploits the two-level approach, in which a relatively small but essential part of the system (*i.e.*, its active site) is simulated at a high quantum-mechanical level, while the remainder is treated at a lower level (for example, using molecular mechanics methods). For instance, the active site of a closed SWNT was simulated by DFT using only 24 carbon atoms [146, 166] (sample No. 13, Table 2).

The first DFT calclulations [147] showed that sorption of hydrogen atoms occurs both inside and outside the SWNT (Fig. 4). Hydrogen atoms adsorbed inside the SWNT can assemble to molecules. Sorption capacity increases linearly with an increase in the diameter of nanotubes. Gravimetric capacity of the system H_2 – (10,10) SWNT † amounts to 14 mass % whereas volume capacity is 160 kg H_2 m^{-3}. Sorption capacity of the system

† The so-called chirality indices of nanotubes (n,m), which define orientation of the axes of a graphene sheet rolled-up into a nanotube with respect to the axes of the tube formed (for details, see, for instance, reviews [12, 15, 16]).

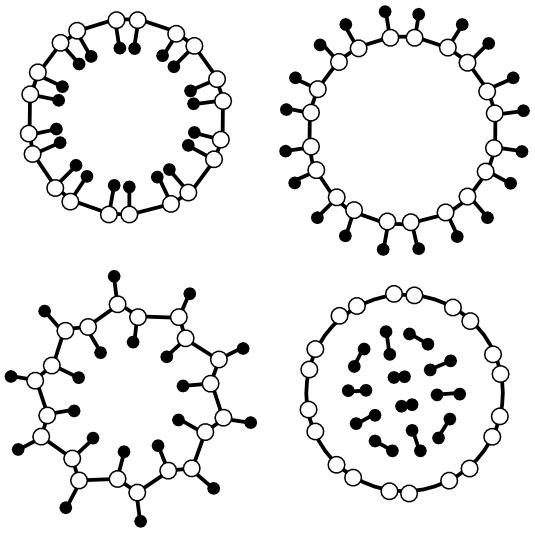


Figure 4. Hydrogen chemisorption centres in SWNT (a model representation, see text).[147]

H_2–MWNT is 7.7 mass % (sample No. 14, Table 2), which is close to the maximum theoretical value.

Bonding energies of an H atom to external surfaces of three types of SWNT, *i.e.*, (9,0), (5,5) (Fig. 5) and (10,0), for their coverage with hydrogen by 50% and 100% were calculated using DFT. It turned out that the hydrogen bonding energies are similar for all the three types of SWNT. For the (10,0) SWNT, another filling pattern, *i.e.*, 50% of H atoms bound to the internal surface and 50% bound to the external surface, was simulated. This filling mode proved to be the optimum one whereas the exclusive filling of the external surface was energetically unfavourable. It remains unclear, to what extent such a model can be achieved in practice, since no methods for the hydrogen insertion and extraction have been developed so far. The authors suggested [146, 166] that these stages can be accomplished using *ad hoc* catalysts initiating cleavage of the H—H and C—H bonds.

Similarly, according to calculations,[167] the system nanotube–H_2 has to be initiated catalytically or electrochemically prior to hydrogen sorption. Hydrogen chemisorption depends on the radius and chirality of the nanotube, as evidenced by the DFT simulation.[167] The threshold radius for the stability of nanotubes with hydrogen adsorbed on their external surface is 0.625 nm [note that it is nanotube (8,8) that have a close radius]. Measurements of photoinduced desorption of hydrogen from SWNT treated with atomic hydrogen [168] confirmed that the critical radii of curvature for chemisorption is $\sim$0.6 nm.

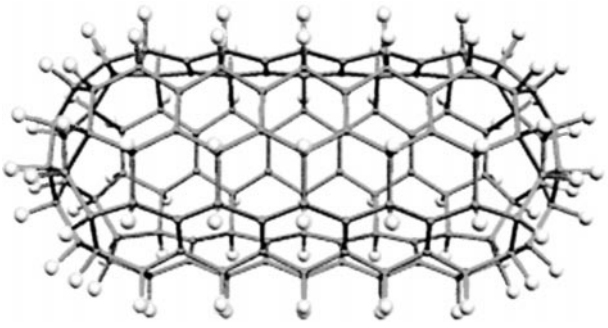


Figure 5. A model of a (5,5) SWNT with 50% coverage (as compared to the ultimate 'carbohydride' filling) with hydrogen (a stable structure).[146, 166]

Calculations at the DFT level have shown that a mechanical deformation of the nanotubes substantially affects the energy of their interaction with hydrogen atoms. An increase in the ellipticity of a nanotube (or a decrease in its radii of curvature) decreases the hydrogen bonding energy to a value typical of hydrogen sorption on a graphene sheet.[163, 169] A certain analogy between hydrogen sorption on a CNT and the basal plane of graphite was derived from *ab initio* calculations [163] (these results will be considered in more detail in the following section).

According to *ab initio* data,[170] dissociative chemisorption of molecular hydrogen from the gas phase on the surface of individual nanotubes is characterised by vanishingly low probability but in the case of a solid phase composed of bundles of nanotubes at a high hydrogen pressure, hydrogen molecules can dissociate forming simultaneously two C—H bonds on adjacent nanotubes. The adsorption is reversible: hydrogen desorbs if the high pressure is released. The experimental studies [19, 78] of hydrogen sorption by arrays of CNT have shown that the complete desorption requires at least 573 K.

In a series of papers,[148–150, 171–173] Ma and coworkers suggested a model describing the interactions of low-kinetic-energy hydrogen atoms (0.5–30 eV) with SWNT based on the molecular dynamics and, partially, *ab initio* calculations. According to their findings, the energy range of 1–3 eV is optimum for the sorption of hydrogen atoms on the external walls of the SWNT; hydrogen atoms with an energy of 4–14 eV are reflected from the walls whereas those with an energy of 16–25 eV are characterised by a high probability of penetrating through the side faces of the closed single-walled nanotubes and accumulating inside these capsules in the form of hydrogen molecules (Fig. 6). Owing to the high mechanical strength of nanotubes, hydrogen molecules can be concentrated therein up to densities exceeding by far that observed upon capillary condensation (sample No. 15, Table 2). According to estimates,[173] pressure of molecular hydrogen embedded into SWNT can reach as high values as 60 GPa. This hydrogen condensate inside individual SWNT, depending on hydrogen density and pressure, can undergo several phase transitions giving rise to different crystal lattices built up of hydrogen molecules.[172] If the pressure of hydrogen inside a (5,5) SWNT is 37.4 GPa, the bulk sorption capacity can reach 0.63 g cm^{-3}, which meets the requirements of the automotive industry. Potential ways to

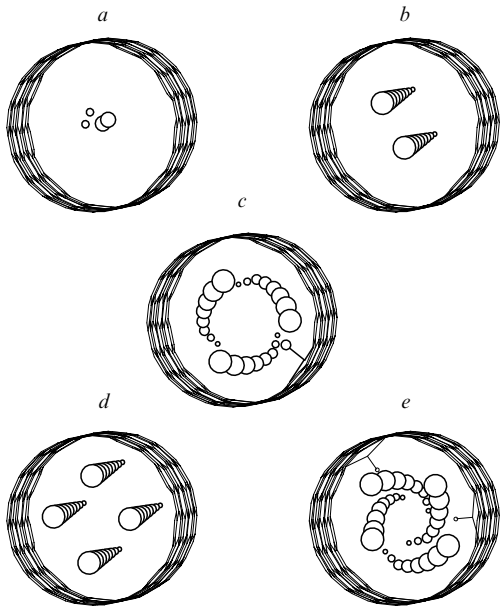


Figure 6. Arrangements of H_2 molecules inside a (5,5) SWNT at different volume densities of hydrogen.[148]
Volume density of hydrogen /kg m^{-3}: (*a*) 20, (*b*) 51, (*c*) 90, (*d*) 125, (*e*) 142.

practical achieving of such high hydrogen sorption levels by bundles of closed SWNT have been suggested as well as methods for hydrogen withdrawal through the walls of the nanotubes.[150, 174]

Recently, the first results of a semi-empirical study on the chemisorption of atomic hydrogen on a graphite sheet with structural defects have been published.[175] The authors used a modified (*i.e.*, not self-consistent) tight-binding model, which, in their opinion, described the chemical bonding between H and C atoms in real complex systems with sufficient accuracy and, at the same time, was simple enough to enable computer simulations.

In general, as correctly pointed out by Froundakis [138] and Tada *et al.*,[176] computer simulations of hydrogen adsorption on carbon nanomaterials conducted so far were successful only in rationalising a few first elementary steps of the overall process. Therefore, any step beyond the bounds of the idealised models would be indeed interesting but its practical implementation is challenging due to the necessity of bulk calculations. A search for conditions that would provide the optimum combination of thermodynamic and kinetic parameters of physisorption and chemisorption, is a current task for the development of hydrogen storage systems.[57, 59]

IV. A thermodynamic analysis of the experimental data

1. Methodology of the analysis

The similarity between the basic chemical structure elements of carbon nanomaterials under consideration and those of graphite implies that their interactions with hydrogen should obey some common rules. In order to elucidate these rules and factors governing the sorption capacities of the respective materials we applied the methods of thermodynamics of reversible processes and formal kinetics (the linear approximation of thermodynamics of irreversible processes). Earlier, we applied this methodology to an analysis of similar problems.[63, 177–180] The proposed methodology includes a new (simplified) procedure [63] for the evaluation of the diffusion coefficient based on the corresponding parameters of the thermodesorption peak and the characteristic length of the diffusion path. The proposed interpretation of the thermodynamic and kinetic (diffusion) parameters calculated in this way takes into account the results of theoretical studies of atomic hydrogen chemisorption by graphite and carbon nanostructures.[163]

2. Solubility, sorption and diffusion of deuterium in isotropic and pyrolytic graphites

Synthetic graphites are usually not single-crystalline materials. They are composed of small polycrystalline granules. One of the models proposed for such a spherical granule of isotropic graphite [181] is shown in Fig. 7. This granule has a size of ~ 2 μm (r_{gg}) and contains crystallite grains with sizes (r_{cg}) ranging from 0.03 μm to 0.2 μm.[182]

The equilibrium solubility of gaseous deuterium in the high-density ($\rho = 1.90$ g cm^{-3}) isotropic graphite ISO-880U (for the measurements, plates with a thickness of $l = 1$ mm were taken) at 1123–1323 K and 2.6–12.7 kPa is described by the following expression (the Sieverts isotherm)

$$x = \frac{D}{C} = 2.0 \times 10^{-7} \left(\frac{P_{D_2}}{P^{\circ}_{D_2}}\right)^{1/2} \exp\left(-\frac{\Delta H}{RT}\right), \quad (1)$$

where $\Delta H = -19 \pm 2$ kJ mol^{-1} is the standard enthalpy of dissolution of 0.5 mol of gaseous deuterium in graphite (the mean value for the above temperature range); P_{D_2} and $P^{\circ}_{D_2}$ are equilibrium and standard pressures of gaseous molecular deuterium at a specific temperature (expressed in Pa), respectively; $P^{\circ}_{D_2} = 1$ Pa.

Making use of the results obtained elsewhere [177, 179, 180] we can show that the expression (1) corresponds to the approximations of the ideal gas phase (hydrogen, deuterium) and the ideal solid solution, for which the infinitely dilute solution ($x^{\circ} \to 0$) can be taken as the standard state. Appropriateness of the approximation for the gas phase (within the temperature and pressure ranges of interest) can be verified using the semi-empirical equations of states for hydrogen.[1, 183] The applicability of the aforementioned approximation for the solid phase (*i.e.*, graphite and carbon nanomaterials) as well as effects of internal stresses and local deformations,[154, 184–187] which emerge upon dissolution of the gas in an inhomogeneous (defect-rich) solid phase, on the apparent solubility of the gas will be considered in the following sections as a part of the experimental data analysis.

Let us first consider the process of deuterium desorption from samples of isotropic graphite with a thickness of 1 mm. In the case of samples of isotropic graphite exposed to deuterium at $P_{D_2} = 60$ kPa and $T = 1173$ K (samples A) or 973 K (samples B) for 5 h, the temperature-programmed desorption curves (TPD) for a heating rate of $\upsilon = 0.17$ K s^{-1} manifest [63, 181] three peaks ‡ (Fig. 8) centred at $T_I \approx 445$ K, $T_{II} \approx 727$ K and $T_{III} \approx 1239$ K and at $T_I \approx 445$ K, $T_{II} \approx 760$ K and $T_{III} \approx 1193$ K for the samples A and B, respectively.

‡ However, one more peak *IV* ($T_{IV} \approx 973$ K) can be revealed, which is especially distinct for the samples deuterated at 673 K and 1173 K (Fig. 8). Also note that two peaks around T_I can be resolved for the samples deuterated at 673 K.

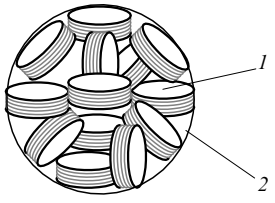


Figure 7. A model of a spherical granule of isotropic graphite [182] composed of independent crystallite grains.
(*1*) A crystallite grain, (*2*) a granule of isotropic graphite.

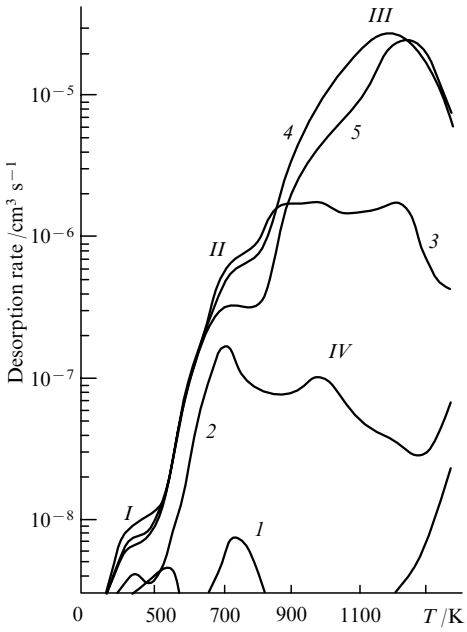


Figure 8. Temperature-programmed desorption of deuterium from isotropic graphite hydrogenated at different temperatures (curves *1* – *5*) (60 kPa, 5 h).[181]
Hydrogenation temperature /K: 473 (*1*), 673 (*2*), 773 (*3*), 973 (*4*) and 1173 (*5*) (for assignment of the TPD peaks *I*–*IV*, see text).

It was suggested [63, 181] that the peak *I* is due to desorption of deuterium molecules adsorbed on the surface of graphite granules, the peak *II* is due to deuterium molecules adsorbed on the surface of crystallite grains and the peak *III* is due to deuterium atoms absorbed (dissolved) in the crystallite grains. This assignment was based on the TPD data [181] obtained for isotropic graphite deuterated at 973 K, which showed that the amount of deuterium (x) desorbed during stages *I* and *II* was proportional to P_{D_2} whereas that desorbed during stage *III* was proportional to $(P_{D_2})^{1/2}$.

Furthermore, the amount of deuterium desorbed from the samples deuterated at 973 K and 60 kPa in the region corresponding to T_{III} was of the same order of magnitude as the equilibrium solubility ($x_{III} \approx 0.6\,x$); the amount of deuterium desorbed in the regions corresponding to T_{II} and T_I was smaller by two and four orders of magnitude, respectively. The equilibrium bulk solubility of deuterium in graphite was achieved only for the samples deuterated at 1173 K and 60 kPa (Fig. 8):[181] $x_{III} \approx x$, $x_{IV} \approx 1.1\times10^{-1}\,x$, $x_{II} \approx 1.5\times10^{-2}\,x$, $x_I \approx 3\times10^{-4}\,x$.

Taking into account that the position of the peak *II* (T_{II}) shifts depending on the thickness of the sample from 760 K (for a sample with a thickness of 1 mm) to 710 K (for a thinner sample with a thickness of $l = 0.45$ mm), annealing of the samples at 573–1173 K has a stepwise character and x_{II} linearly depends on P_{D_2}, Atsumi *et al.*[181] suggested that the peak *II* is due to one-dimensional diffusion of deuterium molecules from the adsorbed nanolayers on the surface of crystallite grains along the nanolayers towards the free external surface of the sample.

The diffusion coefficient as a function of temperature obeys the Arrhenius equation [181]

$$D_{II} = (D_0)_{II}\exp\left(-\frac{Q_{II}}{RT}\right)$$

with a preexponential factor $(D_0)_{II} = 1800$ cm^2 s^{-1} and an activation energy $Q_{II} = 120\pm5$ kJ mol^{-1}.

Taking into account that the peak *III* (in contrast to the peak *II*) does not shift with a decrease in the thickness of graphite samples, annealing of the samples has a stepwise character, x_{III} is proportional to $(P_{D_2})^{1/2}$ (see Ref. 181) and other experimental evidence, in particular, parameters of the bulk diffusion of hydrogen in graphite [188] and data on the sizes of polycrystalline granule grains (r_{gg}) and crystallite grains within these granules (r_{cg}),[108, 181, 182, 189] one may assume that the peak *III* is due to bulk diffusion (*i.e.*, diffusion occuring between the graphene sheets) of deuterium atoms dissolved in graphite crystallite micrograins towards the nearest boundaries of these grains. Temperature dependence of the diffusion coefficient D^*_{III} of hydrogen atoms in crystallite grains of isotropic graphite corrected as compared to the value given by Atsumi *et al.*[181] (see Ref. 188) can be represented in the following form:

$$D^*_{III} = (D^*_0)_{III}\exp\left(-\frac{Q_{III}}{RT}\right),$$

where $(D^*_0)_{III} \approx 3\times10^{-3}$ cm^2 s^{-1}, $Q_{III} = 250\pm10$ kJ mol^{-1}.

It should be stressed that in Ref. 188 (in contrast to Ref. 181) the diffusion coefficient was determined from the experimental data on the characteristic length of diffusion path. Therefore, we find it appropriate to correct the preexponential factor $(D_0)_{III} = 1.7$ cm^2 s^{-1} given in Ref. 181 using the data from Ref. 188. The uncorrected former value corresponds to a mean radius of the polycrystalline granule rather than the crystallite grains. The corrected $(D^*_0)_{III}$ is given by the following formula: $(D^*_0)_{III} = (D_0)_{III}\,(r_{cg}/r_{gg})^{1/2}$.

The characteristic length of diffusion path travelled by a deuterium molecule (L_{II}) corresponding to the peak *II* can be estimated using the following expression:

$$L_{II} \approx (D_{II}\,t)^{1/2} \approx \left(\frac{D_{II}\Delta T_{II}}{\upsilon}\right)^{1/2}, \qquad (2)$$

where $D_{II} = 4.3\times10^{-6}$ cm^2 s^{-1} (for $T_{II} = 727$ K); $t = \Delta T_{II}/\upsilon$ is the diffusion time [$\Delta T_{II} \approx 182$ K is the full width at half maximum of peak *II* (Fig. 8); $\upsilon = 0.17$ K s^{-1} (see Ref. 181)].

Substitution of these values for D_{II} and ΔT_{II} in Eqn (2) gives rise to the value of L_{II}, which agrees with the thickness of the samples (l)§ reported in Ref. 181. In this case, one may consider that the characteristic length of diffusion path (L) was determined experimentally based on the dependence of T_{II} on l.[181]

The apparent sizes of crystallite grains in polycrystalline granules, which correspond to the characteristic length of diffusion path travelled by deuterium atoms from a crystallite grain to its surface (peak *III*), can be estimated using the following expression:

$$L_{III} \approx r_{cg} \approx \left(\frac{D^*_{III}\Delta T_{III}}{\upsilon}\right)^{1/2}, \qquad (3)$$

where $D^*_{III} \approx 1\times10^{-13}$ cm^2 s^{-1} (for $T_{III} = 1239$ K), $\Delta T_{III} \approx 210$ K is the full width at half maximum of the peak *III*. The value of $r_{cg} \approx 0.1$ μm calculated in this way is in accord with the experimental data [108, 182] on the sizes of crystallite grains. These values of structural parameters $r_{cg} \approx 0.1$ μm and $r_{gg} \approx 2$ μm (from Ref. 189) are used below in the analysis and interpretation of the results by Atsumi *et al.*[181]

According to thermodynamic data (for $T \approx 1200$ K), experimental data on equilibrium solubility of deuterium in graphite [$x \approx x_{III} \sim (P_{D_2})^{1/2}, \Delta H$] [181] and diffusion parameters corresponding to the peak *III* [Q_{III}, $(D^*_0)_{III}$, L_{III}], the process of dissolution of gaseous molecular deuterium in graphite crystallite grains can be represented with the following scheme (dissociative chemisorption):[63, 181]

$$0.5\,D_2(\text{gas}) \rightleftharpoons D - 224\ \text{kJ mol}^{-1}, \qquad (4)$$

$$D \longrightarrow D(\text{gr.latt.}), \qquad (5)$$

$$D(\text{gr.latt.}) + C(\text{gr.ch.c.}) \rightleftharpoons DC(\text{gr.abs.}), \qquad (6)$$

$$0.5\,D_2(\text{gas}) + C(\text{gr.ch.c.}) \longrightarrow DC(\text{gr.abs.}) + 19\ \text{kJ mol}^{-1}, \qquad (7)$$

where D is a deuterium atom on the surface of a crystallite grain; D(gr.latt.) is a deuterium atom in the graphite lattice (away from chemisorption centres); C(gr.ch.c.) is an internal carbon chemisorption centre for deuterim in the graphite lattice capable of forming a chemisorbed complex DC; DC(gr.abs.) is a deuterim atom absorbed in the graphite lattice. The total process (7) is characterised by an enthalpy change $\Delta H_{(7)III} = \Delta H \approx -19$ kJ mol^{-1}.

The law of mass action for the reaction (7)

$$K_{III} = \frac{x_{III}/(x_{III})_{max}}{(P_{D_2}/P^\circ_{D_2})^{1/2}[1 - x_{III}/(x_{III})_{max}]} \qquad (8)$$

is transformed into the Sieverts–Langmuir adsorption isotherm:[177, 179]

$$\frac{x_{III}}{(x_{III})_{max}} = \frac{K_{III}(P_{D_2}/P^\circ_{D_2})^{1/2}}{1 + K_{III}(P_{D_2}/P^\circ_{D_2})^{1/2}}, \qquad (9)$$

where equilibrium constant (K_{III}) for the reaction (7) is given by:

$$K_{III} = \exp\left(\frac{\Delta S}{R}\right)\exp\left(-\frac{\Delta H}{RT}\right). \qquad (10)$$

Here, $(x_{III})_{max}$ denotes the maximum possible D/C ratio (or the fraction of internal chemisorption centres), $\Delta H = \Delta H_{(7)III} \approx -19$ kJ mol^{-1}, $\Delta S = \Delta S_{(7)III}$ is the standard change of entropy

§ A similar value $L_{II} \approx l$ is obtained if the diffusion problem is reformulated to an isothermal case (using the value of Q_{II} from Ref. 181).[190, 191]

for the reaction (7). If $x_{III} \ll (x_{III})_{max}$, Eqns (8)–(10) are transformed into the expression (1), *i.e.*, the Sieverts isotherm.

As follows from Eqns (1) and (8)–(10), $(x_{III})_{max} \exp(\Delta S/R) \approx 2 \times 10^{-7}$. For the ultimate (carbohydride) values of concentration $(x_{III})_{max} = 0.5$ (or 1.0),[146] $\Delta S/R \approx -14.7$ (or -15.4), which means that $\Delta S = \Delta S_{(7)III} \approx -122$ (or -128) J K^{-1} mol^{-1} [the latter value is close to the values of ΔS known for reactions similar to (7), see reference books [192–194]]. Within this approximation, the standard enthalpy ($\Delta H_{(7)III}$) and entropy ($\Delta S_{(7)III}$) of absorption for the reaction (7) are independent of the concentration of absorbed deuterium. Note that in this case, it is the concentrated solution ($x^{\circ}/x_{max} = 0.5$) that can be chosen as the standard state for the solid phase, then $\Delta H_{(7)III}$ and $\Delta S_{(7)III}$ in the expression (10) are constants.[177, 179]

Assuming that dissolution of deuterium atoms in the graphite lattice without involvement of chemisorption centres in stage (5) does not modify the enthalpy of the system [*i.e.*, $\Delta H_{(5)III} \approx 0$], the value of enthalpy determined from Eqns (4)–(7) is $\Delta H_{(6)III} \approx -243$ kJ mol^{-1}.

The factors essential for understanding of the mechanism underlying deuterium dissolution in crystallite grains are listed below:

— The calculated value of $\Delta H_{(6)III}$ is close in absolute value to the activation energy of bulk diffusion of deuterium atoms through the graphite crystallite grains but has the opposite sign ($Q_{III} = 250$ kJ mol^{-1}) (see Refs. 181, 188).

— The value of $\Delta H_{(6)III}$ is close to the energy of interaction of hydrogen atoms with the external surface of nanotubes belonging to types (5,5), (10,10), (10,0) and (9,0) calculated using the DFT method.[146, 147]

— The value of $\Delta H_{(6)III}$ is by 48 kJ mol^{-1} larger than the energy of interaction of hydrogen atoms with the graphene surface calculated using the DFT method [195] and the energy of hydrogen sorption on the basal plane of graphite according to the model F (Fig. 9, $\Delta H_F = -195$ kJ mol^{-1}) calculated using the *ab initio* molecular orbitals method.[163] Presumably, the discrepancies between the experimental and theoretical values of $\Delta H_{(6)III}$ are related to large errors associated with theoretical determination of the C–H bonding energy.

Furthermore, estimates for the chemisorption energy of hydrogen on the (0001) basal plane of graphite (models E and F) and on cleaved C–C bonds at (1010) zigzag-like (models D and H) and (1121) chair-like (models C and G) side planes of graphite (Fig. 9)¶ are available, which are sufficiently accurate and can be used to rationalise some parameters of the sorption processes corresponding to peaks *I*–*IV* (see Fig. 8).†

The aforementioned data clearly indicate that both bulk dissolution of D_2 and bulk diffusion of deuterium atoms through the crystallite grains of isotropic graphite (peak *III* in Fig. 8) contribute to the dissociative chemisorption of deuterium on active carbon sites with the absorption enthalpy of $\Delta H_{(abc)III} = \Delta H_{(6)III} \approx -Q_{III}$.

A model [177] of diffusion of hydrogen atoms through the graphite lattice accompanied by reversible capture of the diffusant by internal carbon chemisorption centres yields similar values of the thermodynamic ($\Delta H_{(6)III}$) and kinetic ($-Q_{III}$) parameters of the hydrogen absorption process. In this case, the diffusion activation energy is consumed predominantly to cleavage of the chemisorption bonds formed by the diffusant.

It might be assumed [63] that sorption of two hydrogen atoms on two adjacent centres on the basal plane (model F) generates

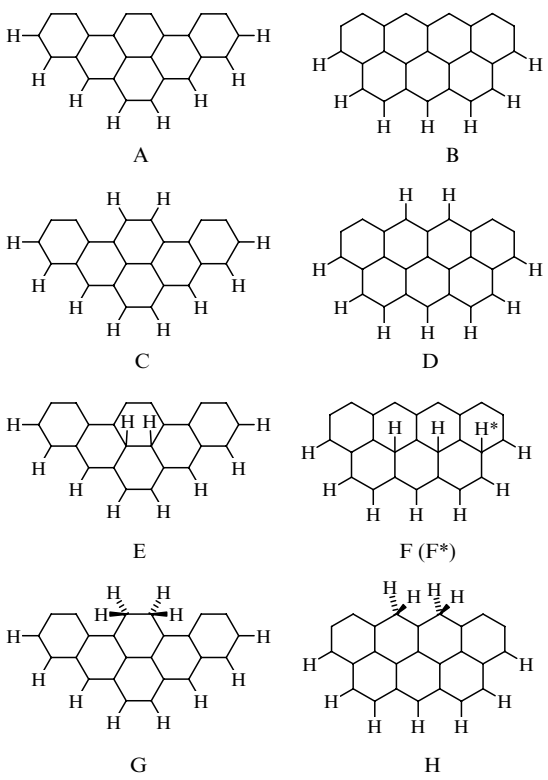


Figure 9. Models of hydrogen chemisorption on graphite (for description of the models, see text).[163]

new potential chemisorption centres for the next hydrogen atoms (third, fourth, *etc.*) on proximate carbon atoms of the graphene layer (model F*, Fig. 9). The energy of chemisorption for the additional hydrogen atoms on adjacent carbon atoms of the graphene layer (model F*) is likely characterised by a value similar to ΔH_F. For the model F*, according to results of Ref. 146 (sample No. 13, Table 2), $(x_{III})_{max} \approx 0.5$ [or $(x_{III})_{max} \approx 1.0$, if both sides of a graphene layer are considered]. The validity of such a model is justified by experimental data on the realisation of a high content of hydrogen isotopes in implanted graphite layers in the case of a-C : H-films (H/C $\approx 0.5-0.7$) [108, 109] and fullerites (H/C $\approx 0.6-0.95$).[19, 103]

Taking into account that the C–H (C–D) chemical bonds are characterised by saturability, directionality and localisation, it might be assumed that the expressions (8) and (9) can remain valid even for deuterium concentrations approaching the ultimate carbohydride values $(x_{III})_{max} \approx 0.5$ (or 1.0). An analysis of the experimental data on the amount of hydrogen isotopes absorbed in nanocrystalline graphite synthesised mechanochemically (see Section IV.6),[27, 29, 30] and on the hydrogen content in graphite nanofibres (see Section IV.9) [32, 33, 196] support the applicability of the model of chemisorption centres and ultimate concentrations $(x_{III})_{max}$ corresponding to a specific bulk carbohydride phase (H/C = 0.5–1.0) [146] to the description of hydrogen sorption by these materials.

Within the model [177] of bulk diffusion of deuterium (hydrogen) atoms through the graphite lattice accompanied by reversible capture of the diffusant by internal chemisorption centres [provided that the predominant fraction of the diffusant is localised in the absorption centres and $x_{III}/(x_{III})_{max} \ll 1$], the apparent diffusion coefficient (D^*_{III}) and activation enthalpy (energy) (Q_{III}) can be written as:

$$D^*_{III} \approx \frac{AD_{latt}}{K_{(6)III}}, \qquad (11)$$

¶ The model A in Fig. 9 corresponds to the basal plane with empty chair-like edge centres, the model B corresponds to the basal plane with empty zigzag-like edge centres.

† A comparison of the experimental values of ΔH (for peaks *I*–*IV*) with the theoretical values of E_{ad} makes it possible the most appropriate model (models C–H, Fig. 9) for description of the sorption process attributed to specific TPD peaks.

$$Q_{III} \approx Q_{\text{latt}} - \Delta H_{(6)III}, \quad (12)$$

where A = const, D_{latt} and Q_{latt} are the diffusion coefficient and the activation enthalpy (energy) for the diffusion of deuterium (hydrogen) atoms through the graphite lattice in the absence of capturing chemisorption centres, respectively; $K_{(6)III}$ is the equilibrium constant of the reaction (6) as applied to peak *III*. Here,

$$D_{\text{latt}} \approx (D_0)_{\text{latt}} \exp\left(-\frac{Q_{\text{latt}}}{RT}\right),$$

$$K_{(6)III} \approx B \exp\left(-\frac{\Delta H_{(6)III}}{RT}\right),$$

where $(D_0)_{\text{latt}}$ and B are preexponential factors.

The activation energy of diffusion of hydrogen atoms in nanostrucured graphite was estimated both experimentally [28] for a temperature range of 300–425 K ($Q_{\text{exp}} \approx 9.6$ kJ mol^{-1}) and theoretically [197] ($Q_{\text{theor}} \approx 1.5$ kJ mol^{-1}). The diffusion activation energy (Q) can be characterised by that small value only if the chemisorption centres are either absent or almost completely occupied, *i.e.*, if $Q = Q_{\text{latt}}$. Provided that Q_{latt} acquires such a value, the activation energy of diffusion of deuterium atoms through the graphite lattice [the expression (12)] approaches the enthalpy of desorption of deuterium atoms from graphite, *i.e.*, $Q_{III} \approx -\Delta H_{(6)III} = -\Delta H_{(\text{abs})III}$.

Taking into account the linear dependence of x_{II} on P_{D_2} and values of Q_{II} (as reported in Ref. 181), it might be assumed that the diffusion processes of deuterium sorption on graphite [181] associated with peak *II* are described by the following reactions:

$$D_2(\text{gas}) \longrightarrow D_2(\text{graph.}), \quad (13)$$

$$D_2(\text{graph.}) \rightleftharpoons 2D(\text{graph.}), \quad (14)$$

$$2D(\text{graph.}) + C(\text{ch.c.}) \rightleftharpoons D_2C(\text{ads.}), \quad (15)$$

$$D_2(\text{gas}) + C(\text{ch.c.}) \longrightarrow D_2C(\text{ads.}), \quad (16)$$

where D_2(graph.) and D(graph.) denote, respectively, a deuterium molecule or atom on the surface of graphite crystallite grains (away from chemisorption centres); C(ch.c.) is a carbon chemisorption centre that binds two deuterium atoms in graphite (potential formation of a D_2C complex) localised at the surface of the crystallite grains; D_2C(ads.) is a couple of deuterium atoms adsorbed on a carbon centre on the surface of the crystallite grains.

Our analysis shows that in many cases the rate of the first stage (13) of the process is diffusion-limited.

There is some evidence (see Refs 28, 197) suggesting that the activation energy for diffusion of deuterium molecules becomes negligibly small as compared to Q_{II} in the absence of chemisorption centres on the surface of crystallite grains.[181] In such a case, the apparent activation enthalpy (energy) for the diffusion of deuterium molecules along the surface of graphite crystallite grains (Q_{II}) should be similar to the standard change of enthalpy for the desorption of deuterium molecules from the surface of crystallite grains, which is the thermodynamic characteristics of a reaction reversed with respect to the reaction (16).

$$\Delta H_{(\text{ads})II} = \Delta H_{(16)II} \approx -Q_{II} = -120 \text{ kJ mol}^{-1}.$$

A similar situation is typical, for instance, of gas chromatography.[198]

The standard change of enthalpy for the reaction (14) at a temperature close to T_{II} can be written as $\Delta H_{(14)} \approx 2\Delta H_{(4)} \approx 450$ kJ mol^{-1} (see Refs 192–194), whereas the standard change of enthalpy for the reaction (15) can be written as $\Delta H_{(15)II} = \Delta H_{(16)II} - \Delta H_{(14)} - \Delta H_{(13)II} \approx -570 \pm 8$ kJ mol^{-1} [provided that $\Delta H_{(13)II} \approx 0$]. The experimentally measured value of $\Delta H_{(15)II}$ is similar to the theoretical value of energy of chemisorption of two hydrogen atoms on a zigzag-like edge carbon centre: $\Delta H_{\text{H}} = -540$ kJ mol^{-1} (model H, Fig. 9).[163] Taking into account that a zigzag-like edge carbon centre cannot adsorb an H_2 molecule, a scheme describing the process of chemisorption of two hydrogen atoms on such a centre should include stages (14) and (15), which correspond to a dissociative-associative adsorption.

The enthalpy of adsorption of deuterium molecules in intergranule nanoareas of graphite can be estimated from the experimental dependence of the area under the peak *I* (that is respective concentration) on deuteration temperature (1173 K and 973 K, Fig. 8) using the Henry adsorption isotherm equation.[181] The standard change of enthalpy for the reaction (16) as applied to the peak *I* is $\Delta H_{(16)I} = \Delta H_{(\text{abc})I} \approx -20 \pm 5$ kJ mol^{-1}, whereas the standards change of enthalpy for the reaction (15) is $\Delta H_{(15)I} = \Delta H_{(16)I} - \Delta H_{(14)} - \Delta H_{(13)I} \approx -465 \pm 7$ kJ mol^{-1} [provided that $\Delta H_{(14)} \approx 445$ kJ mol^{-1} (see Refs 192–194) and $\Delta H_{(13)I} \approx 0$]. The value of $\Delta H_{(15)I}$ obtained in this way is close to the theoretical value of energy of chemisorption of two hydrogen atoms on a chair-like edge carbon centre, which is $\Delta H_{\text{G}} = -480$ kJ mol^{-1} (model G, Fig. 9).[163] Taking into account that the chair-like centre cannot adsorb an H_2 (or D_2) molecule, the stages (14) and (15), which correspond to a dissociative-associative adsorption, should be included in the total chemisorption process.

Probably, any two nearest carbon atoms of graphene layers located at the surface of granules can also act as adsorption centres. Chemisorption of two hydrogen atoms on such a centre is characterised by an energy change of $\Delta H_{\text{F}} = -390$ kJ mol^{-1} (model F, Fig. 9),[163] which is in reasonable agreement with the experimental value of $\Delta H_{(15)I}$.‡ Formally, these centres correspond to potential chemisorbed complexes D_2C_2 (or H_2C_2). Taking this into account, Eqn (15) should be rewritten as:

$$2D(\text{graph.}) + 2\,C(\text{ch.c.}) \rightleftharpoons D_2C_2(\text{ads}). \quad (15a)$$

Since $T_I \ll T_{II}$ and processes associated with peaks *I* and *II* are characterised by identical lengths of diffusion path (L = 1 mm), it might be expected that [according to Eqn (2)] $Q_I < Q_{II}$.[181] The value of Q_I should be close to the standard change of enthalpy of desorption of deuterium molecules from the surface of granules, *i.e.*, $Q_I \approx \Delta H_{(\text{desorb})I} = -\Delta H_{(16)I} \approx 20$ kJ mol^{-1}. Within this formalism, the peak *I* corresponds to diffusion transfer of deuterium molecules from the surface of granules to the external surface of the sample accompanied by their reversible capture by carbon chemisorption centres (to form complexes D_2C or D_2C_2) in nanocavities between granules. The following equations can be applied to calculate the apparent diffusion coefficient of deuterium molecules (D_I) and effective solubility of deuterium ($x_I \approx$ D/C, where C is the total number of carbon atoms in the sample) on the surface of granules:

$$D_I = (D_0)_I \exp\left(-\frac{Q_I}{RT}\right) \approx \frac{AD_{\text{surf}}}{K_{(16)I}}, \quad (17)$$

$$x_I \approx 6\,\frac{\Delta r_I}{r_{\text{gg}}} x_{D_2 I}, \quad (18)$$

$$Q_I \approx -(\Delta H_{(14)I} + \Delta H_{(15)I}) \approx -\Delta H_{(16)I}, \quad (19)$$

$$K_{(16)I} = \frac{x_{D_2 I}/(x_{D_2 I})_{\max}}{(P_{D_2}/P^{\circ}_{D_2})[1 - x_{D_2 I}/(x_{D_2 I})_{\max}]}, \quad (20)$$

$$K_{(16)I} = \exp\left(\frac{\Delta S_{(16)I}}{R}\right)\exp\left(-\frac{\Delta H_{(16)I}}{RT}\right). \quad (21)$$

Here, A = const, D_{surf} is the diffusion coefficient of hydrogen molecules within the surface layer of granules in the absence of chemisorption centres, Δr_I is the effective thickness of the chem-

‡ A similar conclusion was derived from a comparison of the theoretical values of ΔH_{ads} (the models F and F*, Fig. 9) with the experimental values of $\Delta H_{(6)III}$.

isorbing layer on the surface of granules, $x_{D_2 I}$ is the local concentration of D_2 molecules (the ratio D_2/C^*, where D_2 and C^* are numbers of D_2 molecules and carbon atoms in the chemisorbing layer, respectively) on the surface of granules, $(x_{D_2 I})_{max}$ is the maximum concentration of D_2 molecules, $\Delta H_{(14)I}$ and $\Delta H_{(15)I}$ are the standard changes of enthalpy for the reactions (14) and (15), respectively, $\Delta H_{(16)I}$ and $\Delta S_{(16)I}$ are the standard changes of enthalpy and entropy for the reaction (16), respectively, $K_{(16)I}$ is the equilibrium constant for the reaction (16). The equation (20) represents the Henry–Langmuir adsorption isotherm. In the proximity of T_I ($T_I \approx 445$ K), the condition $D_I \approx L_I^2 \upsilon/\Delta T_I$ is met [equation similar to (2)], where $L_I \approx l = 1$ mm (the thickness of the samples).[181] If $x_{D_2 I}/(x_{D_2 I})_{max} \ll 1$, Eqn (20) is reduced to the Henry adsorption isotherm equation.

Substituting $Q_I \approx 20$ kJ mol^{-1} in Eqn (17) and using the expression $D_I \approx L_I^2 \upsilon/\Delta T_I$, one gets $(D_0)_I \approx 3 \times 10^{-3}$ cm^2 s^{-1}.

In order to estimate $x_{D_2 I}$ in the samples of isotropic graphite[181] after their exposure to hydrogen at $P_{D_2} = 60$ kPa and $T = 1173$ K, one can utilise the experimental value of $x_I(D/C) \approx 3 \times 10^{-4} x = 1.0 \times 10^{-7}$. Provided that $r_{gg} \approx 2$ μm and $\Delta r_I \approx$ 0.3 nm, Eqn (18) gives rise to the value $x_{D_2 I} \approx 1.3 \times 10^{-4}$. Within the model G (Fig. 9) for sorption complexes D_2C corresponding to the peak I,[181] it can be taken that $(x_{D_2 I})_{max} \approx 0.5$. Substituting $\Delta H_{(16)I} \approx -20$ kJ mol^{-1} in Eqns (20) and (21), one gets $\Delta S_{(16)I} \approx -180$ J K^{-1} mol^{-1} [the latter value is typical of chemical reactions similar to (16)[192–194]]. It might be assumed that for the D_2C_2 centres of type F (Fig. 9) at $(x_{D_2 I})_{max} \approx 0.25$, $\Delta S_{(16)I} \approx -170$ J K^{-1} mol^{-1}.

The respective expressions for the desorption process corresponding to the peak II can be written as:

$$D_{II} = (D_0)_{II} \exp\left(-\frac{Q_{II}}{RT}\right) \approx \frac{A' D'_{surf}}{K_{(16)II}}, \quad (22)$$

$$x_{II} \approx 6 \frac{\Delta r_{II}}{r_{cg}} x_{D_2 II}, \quad (23)$$

$$Q_{II} \approx -(\Delta H_{(14)II} + \Delta H_{(15)II}) \approx -\Delta H_{(16)II}, \quad (24)$$

$$K_{(16)II} = \frac{x_{D_2 II}/(x_{D_2 II})_{max}}{(P_{D_2}/P^{\circ}_{D_2})[1 - x_{D_2 II}/(x_{D_2 II})_{max}]}, \quad (25)$$

$$K_{(16)II} \approx \exp\left(\frac{\Delta S_{(16)II}}{R}\right) \exp\left(-\frac{\Delta H_{(16)II}}{RT}\right), \quad (26)$$

where respective parameters have similar physical meanings to those in the formulas (17)–(21) but correspond to peak II and $\Delta H_{(16)II} \approx -Q_{II} = -120$ kJ mol^{-1}.

Using the experimental value $x_{II} \approx 1.5 \times 10^{-2} x = 5.2 \times 10^{-6}$ and assuming that $r_{cg} \approx 0.1$ μm and $\Delta r_{II} \approx 0.3$ nm, one gets from Eqn (23) that $x_{D_2 II} \approx 4.0 \times 10^{-4}$. Similarly, using the values $\Delta H_{(16)II} \approx -120$ kJ mol^{-1} and $(x_{D_2 II})_{max} \approx 0.5$, one gets from Eqns (25) and (26) that $\Delta S_{(16)II} \approx -250$ J K^{-1} mol^{-1}.

According to our analysis, parameters of sorption and diffusion of deuterium in isotropic graphite,[181] which correspond to the peak IV (Fig. 8) are in satisfactory agreement with the respective parameters of sorption and diffusion of tritium in pyrolytic graphite§ (data from the review by Causey[109]).

In particular, the apparent enthalpy of activation of tritium diffusion[109] ($Q = 365 \pm 50$ kJ mol^{-1}) is close in absolute value (but opposite in sign) to the theoretical value of energy of chemisorption of a hydrogen atom on a chair-like ($\Delta H_C = -360$ kJ mol^{-1}, model C, Fig. 9)[163] or zigzag-like ($\Delta H_D = -380$ kJ mol^{-1}, model D, Fig. 9) edge carbon centre. The experimentally measured value of tritium dissolution enthalpy[109] ($\Delta H \approx -140$ kJ mol^{-1}) is close to the value of ΔH calculated for the reactions (4)–(7) based on the models C and D assuming that $\Delta H_{(4)} \approx 228$ kJ mol^{-1}: $\Delta H = \Delta H_{(7)IV} \approx \Delta H_{(4)} + \Delta H_{C(D)} \approx -132$ kJ mol^{-1} and -152 kJ mol^{-1} for the models C and D, respectively (see Refs 192–194). Thus, the experimental results[109] can be interpreted on the basis of Eqns (4)–(12) for the chemisorption centres belonging to types C and D (Fig. 9).

Assuming that the experimental data[181] corresponding to the peak IV (Fig. 8) for isotropic graphite can be described in a similar way, one can write:

$$\Delta H_{(7)IV} \approx \Delta H_{(4)} + \Delta H_{(6)IV}, \quad (27)$$

$$Q_{IV} \approx Q_T \approx -\Delta H_{(6)IV} \approx -\Delta H_C \approx -\Delta H_D, \quad (28)$$

where $\Delta H_{(7)IV}$ and $\Delta H_{(6)IV}$ are the standard enthalpy changes for the reactions (7) and (6) as applied to peak IV (Fig. 8); Q_{IV} is the apparent activation enthalpy (energy) for the diffusion process.

The effective diffusion coefficient of deuterium (tritium) atoms in graphite corresponding to the peak IV can be calculated according to the following equation:

$$D_{IV} \approx D_T = (D_0)_{IV} \exp\left(-\frac{Q_{IV}}{RT}\right),$$

where $(D_0)_{IV} \approx 620$ cm^2 s^{-1}, $Q_{IV} \approx Q_T \approx 365$ kJ mol^{-1} (data from Ref. 109).

For the graphite samples,[181] the desorption peak IV is characterised by the following values of parameters (Fig. 8): $T_{IV} \approx 973$ K, $\Delta T_{IV} \approx 140$ K, $x_{IV} \approx 0.11x \approx 3 \times 10^{-5}$. Substituting these values into the equation

$$L_{IV} \approx \left(\frac{D_{IV} \Delta T_{IV}}{\upsilon}\right)^{1/2}$$

it is possible to estimate the characteristic length of diffusion path of deuterium atoms ($L_{IV} \approx 1$ nm).

Sorption and diffusion parameters of the process corresponding to the peak IV are described by equations analogous to Eqns (8)–(12) for the peak III, thus giving rise to

$$\Delta S = \Delta S_{(7)IV}, \Delta H = \Delta H_{(7)IV} \approx -140 \text{ kJ mol}^{-1},$$

$$\Delta H_{(6)IV} \approx \Delta H_{C(D)} \approx -370 \text{ kJ mol}^{-1},$$

$$x_{IV} \approx \left(\frac{3 L_{IV}}{r_{cg}}\right) x_{DIV},$$

where x_{DIV} is the local concentration of deuterium atoms (D/C) absorbed in the graphite layer with the thickness L_{IV} in the proximity of boundaries of the crystallite grains, $(x_{DIV})_{max} \leqslant 0.5$.

It should be noted that the parameters calculated in this way for the peak IV (Fig. 8) require further refinement. However, even within the current approximation they give satisfactory explanation for the abrupt slowing-down of the diffusion process[181] upon isothermal deuteration of isotropic graphite at 473–773 K and 60 kPa as compared to the rate of deuterium desorption upon annealing of the samples hydrogenated at 973–1173 K extrapolated to the respective temperatures (Fig. 8).

In order to refine the parameters of the TPD peaks I–IV (Fig. 8) it would be reasonable to analyse a large array of the experimental data on sorption and diffusion of hydrogen in various graphite materials including graphite layers ion-implanted with hydrogen followed by neutron irradiation and a-C : H films.[108, 109]

Typically, absorption of hydrogen in graphite, *i.e.*, dissolution of hydrogen atoms in the graphite lattice (a bulk phenomenon) is contrasted[100] to hydrogen chemisorption on cleaved σ-bonds on the surface of the crystal, grain boundaries and dislocations

§ Pyrolytic graphite is routinely synthesised by pyrolysis of hydrocarbons. Depending on the experimental conditions and composition of the starting gas, crystals with different sizes and orientations can be prepared.

Table 3. Basic results of the analysis of data on sorption and diffusion of hydrogen (deuterium) in isotropic [181] and pyrolytic [109] graphites.

Experimental data (Fig. 8)	Models of		Reactions	Parameters of processes		Equations used for the calculations	Type of the adsorption isotherm
	sorption (Fig. 9)	diffusion		sorption	diffusion		
Peak *III*	Dissociative chemisorption (model F*)	Diffusion of deuterium atoms through the crystallite grains	(4)–(7)	$\Delta H = \Delta H_{(7)III} \approx -19$ kJ mol^{-1}, $\Delta S/R \approx -14.7$ (-15.4) for $(x_{III})_{max} = 0.5$ (1.0)	$(D_0^*)_{III} \approx 3 \times 10^{-3}$ cm^2 s^{-1}, $Q_{III} \approx$ 250 kJ mol^{-1}	(3), (8)–(12)	Sieverts–Langmuir [Eqns (8), (9)]
Peak *II*	Dissociative–associative chemisorption (model H)	Diffusion of deuterium molecules along the boundaries of the crystallite grains	(13)–(16)	$\Delta H_{(16)II} \approx -120$ kJ mol^{-1}, $\Delta S_{(16)II}/R \approx -30.0$ for $(x_{D_2II})_{max} = 0.5$	$(D_0)_{II} \approx$ 1800 cm^2 s^{-1}, $Q_{II} \approx$ 120 kJ mol^{-1}	(2), (22)–(26)	Henry–Langmuir [Eqn (25)]
Peak *I*	Dissociative-associative chemisorption (models G and/or F)	Diffusion of deuterium molecules along the boundaries of the granules	(13)–(16)	$\Delta H_{(16)I} \approx -20$ kJ mol^{-1}, $\Delta S_{(16)I}/R \approx -21.3$ for $(x_{D_2I})_{max} = 0.5$	$(D_0)_I \approx 3 \times 10^{-3}$ cm^2 s^{-1}, $Q_I \approx$ 20 kJ mol^{-1}	(17)–(21)	Henry–Langmuir [Eqn (20)]
Peak *IV*	Dissociative chemisorption (models C and/or D)	Diffusion of deuterium and tritium atoms through the intergrain nanoregions	(4)–(7)	$\Delta H_{(7)IV} \approx -140$ kJ mol^{-1}	$(D_0)_{IV} \approx$ 620 cm^2 s^{-1}, $Q_{IV} \approx$ 365 kJ mol^{-1}	(27), (28)	Sieverts–Langmuir [Eqns (8), (9)]

(surface phenomena). For this, it should be stressed that the peak *III* for isotropic graphite (see Fig. 8) corresponds to chemisorption of hydrogen atoms on the internal carbon centres located at the graphite ¶ basal planes.

The process of desorption [stage (6)] of single hydrogen (or deuterium) atoms dissolved between the graphene sheets within the graphite crystallite grains [181] corresponding to the peak *III* is not accompanied by abstraction of carbon atoms from the graphene sheets, since the desorption energy of a hydrogen atom [$-\Delta H_{(6)III} \approx 243$ kJ mol^{-1}] is three times smaller than the energy required to abstract a carbon atom from its three carbon neighbours in a graphene layer [$-3/2\,\Delta H_{(C-C)} \approx 730$ kJ mol^{-1}, model F*, Fig. 9].

In the case of peaks *I* and *IV* for graphite,[181] the desorption energy of hydrogen atoms [stages (15) or (6) $-\Delta H_{(15)I} \approx$ 465 kJ mol^{-1} (models G, F) or $-\Delta H_{(6)IV} \approx 370$ kJ mol^{-1} (models C, D)] are also smaller than the energy required to abstract a carbon atom from its neighbours (485 kJ mol^{-1} or 1460 kJ mol^{-1} for the peak *I* and 485 kJ mol^{-1} for the peak *IV*).

The opposite situation is observed in the case of the desorption of two hydrogen (deuterium) atoms adsorbed on the surface of the graphite crystallite grains [stage (15)][181] corresponding to the peak *II*, since the desorption energy of two hydrogen atoms [$-\Delta H_{(15)II} \approx 570$ kJ mol^{-1}, model H, Fig. 9] is larger than the abstraction energy of a carbon atoms from its two neighbours (485 kJ mol^{-1}). In this case, the desorption of hydrogen atoms can be accompanied by abstraction of carbon atoms followed by formation and desorption of hydrocarbon molecules (CH_4, C_2H_4, *etc*.).

* * *

This is supported by mass-spectrometric data,[181] which reveal concomitant liberation of methane (CD_4) from hydrogenated graphite samples. The total amount of liberated methane is three orders of magnitude smaller than the total amount of desorbed deuterium and constitutes ~10% of deuterium desorbed at T_{II}. Liberation of small amounts of hydrocarbons has also been detected in the course of hydrogen desorption from nanostructured graphite and carbon nanofibres (see Sections IV.6 and IV.9).

Thus, the following equation should be utilised in order to determine the effective deuterium (hydrogen) concentration in isotropic graphite [181] hydrogenated at a temperature and exposure sufficiently high to achieve the equilibrium state both inside the crystallite grains and granules and at their boundaries:

$$x_\Sigma(\mathrm{D/C}) = x_I + x_{II} + x_{III} + x_{IV}. \quad (29)$$

Relaxation times (τ_I, τ_{II}, τ_{III}, τ_{IV}) of diffusion processes corresponding to the TPD peaks *I*–*IV* for graphite [181] can be estimated on the basis of D_I, D_{II}, D^*_{III}, D_{IV} and characteristic lengths of diffusion path L_I, L_{II}, L_{III} and L_{IV}.

The major results concerning the analysis and interpretation of data on the sorption of hydrogen in isotropic [181] and pyrolytic [109] graphites are summarised in Table 3. These results are used below to analyse and rationalise some published data on hydrogen sorption by other carbon nanomaterials.

3. High-temperature sorption and diffusion of hydrogen in nanoporous carbon

This section analyses experimental data [67, 199, 200] on high-temperature hydrogen sorption by nanoporous carbon (NPC) composed of graphite-like microfragments joined together by a pyrocarbon binder.

The overall porosity of one of the investigated materials [67] reached ~70% (~40% of porosity was due to nanopores with a mean diameter of ~0.8 nm and the remaining 30% of porosity was due to pores with sizes in the range 0.2–1 μm), specific surface area of this sample (S_{sp}) was ~1200 m^2 g^{-1}.

For the temperature-programmed desorption measurements,[199] samples with a thickness of $l = 1$ mm (exposed to hydrogen at $P_{H_2} = 7.1$ MPa and $T = 523$ K for 3 h) were heated at a rate of $\upsilon = 7.5 \times 10^{-2}$ K s^{-1}. The TPD curves manifest three peaks (Fig. 10) centred at 753 K (peak *I*′), 923 K (peak *II*′) and 1193 K (peak *III*′). The total hydrogen concentration x_Σ in the studied samples was up to 0.16.

The peak *I*′ is comparable in its origin and parameters of the sorption and diffusion processes to those of the peak *II* (Table 3)

¶ Essentially, chemisorption can be involved also in the cases of nanostructured graphite and carbon nanofibres. For high concentrations of chemisorbed hydrogen in such materials, the interlayer separation between graphite layers is substantially increased, which is supported by the experimental X-ray diffraction data (see Sections IV.6 and IV.9).

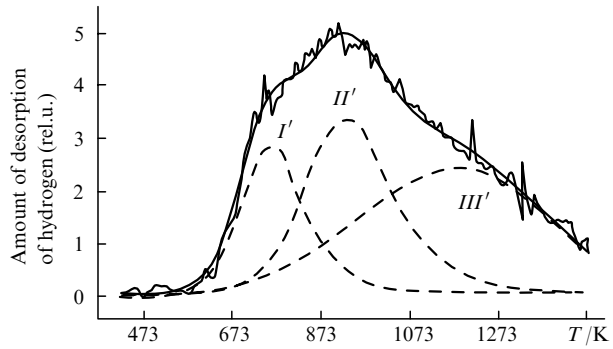


Figure 10. Temperature-programmed desorption of hydrogen from nanoporous carbon hydrogenated at 523 K and P_{H_2} = 7.1 MPa for 3 h (for assignment of the TPD peaks, see text).[199]
The experimental curve shown as a solid line, its components are shown as dashed lines.

for isotropic graphite discussed above.[181] Substitution of the experimental values of $T_{I'}$, $D_{II}(T_{I'})$, υ and $\Delta T_{I'}$ into Eqn (2) yields the length of diffusion path of hydrogen molecules ($L_{I'} \approx 1$ mm), which is in agreement with the thickness of the samples.[199] The hydrogen concentration corresponding to the peak I' [$x_{I'} \approx x_\Sigma(S_{I'}/S_\Sigma) \approx 0.04$] can be described with the expression (23) as well as expressions (25) and (26) (for 523 K and 7.1 MPa). Assuming $x_{II} \approx x_{I'}$ and $\Delta r_{II} \approx 0.3$ nm, the mean size (radius) of a nanograin in the NPC samples can be estimated as $r_{cg} \approx 10$ nm.[199]

The peak II' on the TPD curve for hydrogen desorption from NPC [199] is analogous to the peak *III* (Table 3) for isotropic graphite.[181] The mean size of nanograins for the NPC samples [199] estimated using Eqn (3) is 4 nm ($L_{III'}$) in satisfactory agreement with the aforementioned value of r_{cg}. The concentration of hydrogen corresponding to the peak II' [$x_{II'} \approx x_\Sigma(S_{II'}/S_\Sigma) \approx 0.06$] can be described using the expressions (8)–(10) (for 523 K and 7.1 MPa).

Presumably, the peak III' for NPC (see Ref. 199) is analogous to the peak *IV* (Table 3) for isotropic graphite.[181] Based on the equation similar to (3) and experimental values of $T_{III'}$, $D_{IV}(T_{III'})$, υ and $\Delta T_{III'}$, a value $L_{III'} \approx 190$ nm can be derived, which should characterise the mean linear size of areas of localisation of the corresponding chemisorption centres in the NPC samples.[199]

4. Parameters of hydrogen diffusion in nanostructured pyrolytic graphite

Recently,[68, 69, 201] experimental results on hydrogen thermodesorption from highly oriented pyrolytic graphite [108] exposed to atomic hydrogen at 323–363 K have been reported. This treatment resulted in emergence of surface nanohillocks with heights of 3–5 nm and diameters of 40–75 nm, which can be considered as a sort of nanostructuring of graphite. The nanohillocks disappeared after hydrogen desorption that proceeded as a first-order reaction.[69, 201] Probably, the nanohillocks are formed due to filling of nanocavities with gaseous molecular hydrogen at a high pressure ($P_{H_2} \approx 30$–50 MPa [68]). The TPD measurements (at a heating rate of υ = 25 K s^{-1}) revealed [69, 201] two dominant peaks: a peak α centred at $T_\alpha \approx 1123$ K ($\Delta T_\alpha \approx 180$ K, $S_\alpha/S_\Sigma \approx 0.45$, the activation energy of the process is $Q_\alpha \approx 230$ kJ mol^{-1}) and a peak β centred at $T_\beta \approx 1523$ K ($\Delta T_\beta \approx 250$ K, $S_\beta/S_\Sigma \approx 0.55$, $Q_\beta \approx 385$ kJ mol^{-1}).

The peak α can be attributed to bulk diffusion of hydrogen atoms dissolved in graphite through the nanocavities towards the external free surface of the samples.[68] It should be correlated with the peak *III* for isotropic graphite.[181] The length of the diffusion path (which, in this case, means the width of the nanocavity) is calculated based on Eqn (3), $L_\alpha \approx 4$ nm.

The peak β is analogous to the peak *IV* for isotropic graphite.[181] Using Eqn (3), the length of the diffusion path can be estimated as $L_\beta \approx 300$ nm, this value, effectively, characterises the mean linear size of the areas of localisation of the corresponding chemisorption centres in the samples.[69, 201]

5. Parameters of hydrogen diffusion and sorption in films of nanostructured carbon

Let us now consider experimental data [104, 105] on hydrogen sorption by films of nanostructured carbon prepared using ultrasound-assisted deposition of carbon clusters. The films had porous structures where the size distribution of pores peaked at 3.4 nm and the specific surface area of the samples was 665 m^2 g^{-1} (while volume of the samples was $\sim$0.9 mm^3). The samples hydrogenated at $T \approx 298$ K and P_{H_2} = 100 kPa revealed two dominant peaks in TPD (measured with a heating rate of υ = 0.33 K s^{-1}) with the following characteristics: peak α ($T_\alpha \approx 513$ K, $\Delta T_\alpha \approx 220$ K, $x_\alpha \approx 6 \times 10^{-2}$) and peak γ ($T_\gamma \approx 970$ K, $\Delta T_\gamma \approx 150$ K, $x_\gamma \approx x_\alpha$).

These values assume that peaks α and γ for nanostructured carbon [104, 105] are analogous to peaks *II* and *III* for isotropic graphite.[181] The lengths of diffusion path for hydrogen molecules and atoms can be derived from Eqns (2) and (3). The values obtained in this way, $L_\alpha \approx 9$ μm and $L_\gamma \approx 3$ nm, most probably characterise the mean thickness of the film [104, 105] and the size of the crystallite grains, respectively. The expressions (9), (10), (23), (25) and (26) (for $\sim$298 K and 100 kPA) give rise to the values of $x_{III} \approx 0.1$, which is close to x_γ, and the characteristic size of the crystallite grains $r_{cg} \approx 10$ nm, which is close to L_γ.

* * *

The analysis conducted above indicates that the parameters and equations (Table 3) proposed for characterisation of processes of hydrogen desorption from isotropic graphite [181] give a satisfactory description of the processes corresponding to analogous TPD peaks for a range of nanostructured carbon materials.[67–69, 104, 105, 199–201]

6. Parameters of hydrogen diffusion and sorption in mechanochemically synthesised nanocrystalline graphite

Let us now turn to experimental data [27, 29, 30] on hydrogen and deuterium sorption by mechanochemically synthesised nanocrystalline graphite. The starting material [27, 29] represented graphite powder composed of microgranules with a diameter of $l_{mg} \approx 200$ μm. The graphite powder was saturated with hydrogen (or deuterium) during its milling in a ball mill for 80 h at $T \approx 300$ K and $P_{H_2(D_2)}$ = 1.0 MPa. As a result, a material containing $x_\Sigma \approx 0.96$ of hydrogen was produced. The specific surface area of this sample after milling for 80 h was $S_{sp} \approx 10$ m^2 g^{-1}, which was close to its starting value.[27] For the graphite microgranules after milling for 2 hours, the linear size of nanocrystallites in the direction perpendicular to the graphene layers estimated from the width of peak (002) in the diffraction pattern was $l \approx 40$ nm.[29] The linear size of nanocrystallites ('nanograins') along the graphene layers for the microgranules after milling for 20–80 h was $l_{cg} \leqslant 4$ nm according to Raman scattering and neutron diffraction data.[29] The TPD curves measured for desorption of hydrogen (or deuterium) from these samples upon heating at a rate of υ = 0.33 K s^{-1} revealed two peaks (Fig. 11): a peak α ($T_\alpha \approx$ 730 K, $\Delta T_\alpha \approx$ 130 K, $S_\alpha/S_\Sigma \approx$ 0.8–0.6) and a peak β ($T_\beta \approx 1000$ K, $\Delta T_\beta \approx 30$ K, $S_\beta/S_\Sigma \approx 0.2$–$0.4$). Minor desorption peaks of hydrocarbons with masses of 16 (CH_4) and 28 (C_2H_4) were also detected [29] around T_α (Fig. 11 *a*). No extra peaks were detected around T_β. It is noteworthy that the peak β appears at the same temperature as the peak observed by differential thermal analysis (DTA) and attributed to recrystallisation of nanostructured graphite, which is characterised by the activation enthalpy of $Q_{recr} \approx 244$ kJ mol^{-1}.

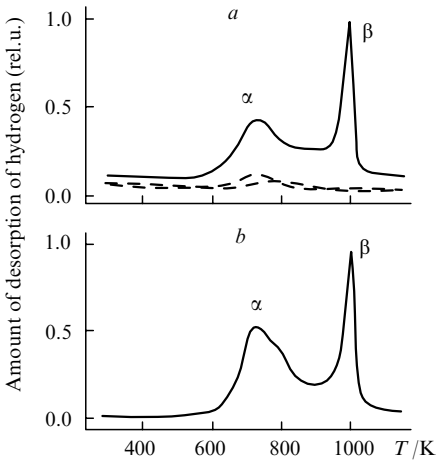


Figure 11. Temperature-programmed desorption of hydrogen (*a*) and deuterium (*b*) (solid lines) from nanocrystalline graphite saturated with hydrogen (or deuterium) during mechanochemical synthesis (1.0 MPa, 300 K, 80 h).[29]
The desorption curves of CH_4 and C_2H_4 are shown as dashed lines.

On the basis of neutron diffraction and Raman scattering data, Orima *et al.* suggested[27,29,30] that the peak α is due to desorption of chemically bound hydrogen (deuterium) whereas the peak β is due to desorption of hydrogen (deuterium) from the interlayer space of the crystallite grains. Therefore, peak β is analogous to peak *III* for isotropic graphite.[181] The length of diffusion path, which corresponds to the linear size of the crystallite grains or nanograins (l_{cg}), determined using Eqn (3) is $L_\beta \approx 2$ nm. This value agrees with the value $l_{cg} \leqslant 4$ nm found experimentally[29].

The calculated concentration of hydrogen $x_\beta \approx (S_\beta/S_\Sigma)x_\Sigma \approx 0.2-0.4$ is in agreement with the value $x_{III} \approx 0.2-0.3$ determined using Eqns (9) and (10) at $P_{D_2} = 1$ MPa and $T = 300$ K, which assumes that under the experimental conditions, the equilibrium bulk solubility of hydrogen (deuterium) in the graphite lattice is reached.[27,29]

The experimental and calculated values of bulk solubility of hydrogen (deuterium) in the graphite lattice[27,29] ($x_\beta \approx x_{III} \approx 0.2-0.4$) approach the ultimate (carbohydride) values of concentrations of occupied chemisorption DC centres in the graphene layers (Table 3).

Evidently, the peak α is due to diffusion of hydrogen (deuterium) molecules from the surface of the crystallite grains towards the external surface of the granules, *i.e.*, it corresponds to the peak *II* (Table 3) for isotropic graphite.[181]

The length of diffusion path L_α estimated using Eqn (2) is comparable to the diameter of graphite microgranules ($l_{mg} \approx 200$ μm) within the samples.[27,29]

The local concentration of hydrogen (deuterium) molecules $x_{D2\alpha}$ on the surface of the crystallite grains can be calculated using the following formula:

$$x_\alpha \approx 12\left(\frac{\Delta r}{l_{cg}}\right)x_{D_2\alpha}\,, \qquad (23a)$$

and the value $x_\alpha \approx (S_\alpha/S_\Sigma)x_\Sigma \approx 0.6-0.8$. Substitution of $\Delta r \approx 0.3$ nm and $l_{cg} \approx 3$ nm[29] in (23a) gives rise to the value of $x_{D2\alpha}$, which is close to the ultimate values of concentration of the chemisorption centres D_2C (model H, Fig. 9), which correspond to formation of a carbohydride adsorbed nanophase on the surface of the crystallite grains.

The above results, in particular, imply that the nanoareas at boundaries of the crystallite grains in nanostructured graphite[27,29] are similar to a certain extent to those of the crystallite micrograins in polycrystalline microgranules of isotropic graphite.[181]

It would be useful to note that such nanoareas at boundaries of crystallite grains are evidently formed upon milling of graphite[27,29] in a ball mill, *i.e.*, upon periodic high-speed plastic deformation of graphite, which results[178] in emergence of a high stationary dislocation density in the material being deformed. These dislocations apparently accelerate diffusion mass transfer of hydrogen in grapite during mechanochemical synthesis of these materials in the atmosphere of hydrogen.[27,29]

Kinetics of hydrogenation of graphite milled in a ball mill (*i.e.*, synthesised mechanochemically) can be formally described as a first-order reaction (Fig. 12):[63,178,202]

$$x_{\Sigma(t)} \approx x_{\Sigma 0}\left[1 - \exp\left(-\frac{t}{\tau_\Sigma}\right)\right]. \qquad (30)$$

Here, $x_{\Sigma(t)}$ is the mean deuterium concentration in the material subjected to milling (mechanochemical synthesis) for a time t; $x_{\Sigma 0}$ is the saturation concentration of deuterium in nanocrystalline graphite; τ_Σ is the relaxation time of diffusion process within the material during mechanochemical hydrogenation ($\tau_\Sigma \approx L_\Sigma^2/D_\Sigma$), where L_Σ is the distance travelled by deuterium in graphite upon mechanochemical synthesis, D_Σ is the apparent deuterium diffusion coefficient in graphite, $\tau_\Sigma \approx 16$ h. This yields a value $D_\Sigma \approx (L_\Sigma^2/\tau_\Sigma)$ that is larger by many orders of magnitude than D^*_{III} and by several orders of magnitude than D_{II}, estimated using the respective equations (see Table 3). Therefore, deuterium diffusion in graphite is abnormally accelerated during mechanochemical synthesis.

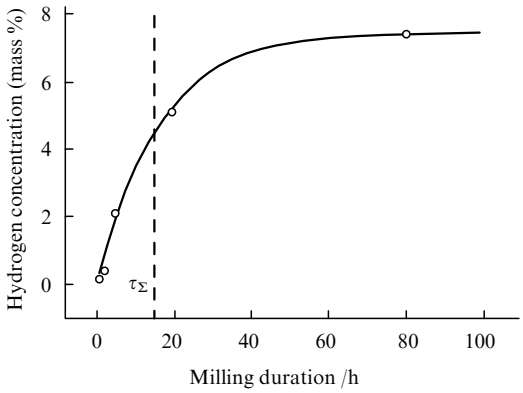


Figure 12. The kinetics of hydrogenation of nanostructured graphite during mechanochemical synthesis [$P_{D_2(H_2)} = 1$ MPa, $T = 300$ K].[27,29]

A series of samples of mechanochemically nanostructured graphite[27,28,124] hydrogenated up to $x_\Sigma \approx 0.96$ (according to Ref. 28) and $x_\Sigma \approx 0.24$, 0.31 and 0.96 (according to Ref. 124) has been studied using NMR. NMR spectra of the samples with $x_\Sigma \approx 0.96$ manifested two peaks suggestively attributed[27,28,124] to chemisorption of deuterium on defect areas (peak *1*) and physisorption of deuterium in the interlayer space (peak *2*).

Additionally, spin–lattice relaxation times of hydrogen atoms were measured[28,124] for the samples of mechanochemically nanostructured graphite (with $x_\Sigma \approx 0.96$, 0.31, 0.24) at 67.7 MHz in a temperature range of 300–425 K (the peak had the maximum intensity at ~390 K). Based on these experimental data, the enthalpy of activation of hydrogen diffusion in graphite (ΔH_a) was estimated as 9.6 kJ mol^{-1}. The authors attributed this 'suprisingly low' value of H_a to diffusion of hydrogen physisorbed between the graphene layers.

Taking into account the specific character of the NMR procedure utilised in the above studies[28,124], theoretical results (MD simulation)[197] concerning hydrogen diffusion between the graphene layers (in the absence of chemisorption centres) as well as the results of our analysis of published data,[27,29,30] it might be

assumed that the above value $\Delta H_a \approx 9.6$ kJ mol^{-1} characterises the enthalpy of activation [Q_{latt} in Eqn (12)] of diffusion of those hydrogen atoms located between the graphene layers, which have not been captured by the chemisorption centres. There are some reasons to suggest that the chemisorption centres capable of capturing the diffusant appeared completely occupied (up to the ultimate hydrocarbon concentrations H/C $\approx$ 1) under the experimental conditions.[28] This situation is equivalent to the lack of the chemisorption centres.[177, 203] The diffusion coefficient determined under such conditions should be close to D_{latt} [expression (11)]. Furthermore, it might be suggested that peaks *1* and *2* in the NMR spectra [28, 124] characterise the same processes as TPD the peaks α and β, respectively.[29, 31]

7. Hydrogen sorption and diffusion in bundles of single-walled carbon nanotubes

Hydrogen sorption by soot containing ~0.01 mass % – 0.02 mass % of SWNT bundles has been studied.[18] The bundles were composed of 7 – 14 SWNT (each tube had a diameter of ~ 1.2 nm and a length of ~ 5 μm). The soot samples (with a mass of ~1 mg) were exposed to hydrogen for 10 min at $P_{H_2} = 40$ kPa and $T = 273$ K (followed by quenching for 3 min at 133 K), then they were heated at a rate of $\upsilon = 1$ K s^{-1}. The TPD curves revealed two peaks (α and β) centred at ~150 K (peak α) and ~288 K (peak β characterised by the following parameters: $\Delta T_\beta = 50$ K, $x_\beta \approx 0.6 - 1.2$).† Based on additional TPD measurements with $\upsilon = 0.3 - 30$ K s^{-1}, the activation enthalpy of the process was determined ($Q_\beta = 19.6$ kJ mol^{-1}, peak β) according to the Kissinger procedure. The process was considered to be a first-order reaction.

The similarity between Q_β and Q_I (see Table 3) allows one to suggest that the diffusion process corresponding to the peak β is analogous to that attributed to the peak *I* for isotropic graphite.[181] Therefore, in order to estimate the length of diffusion path, Eqn (2) can be used, which yields $L_\beta \approx 70$ μm. This value is close to the thickness of the sample. Evidently, in this case, diffusion of hydrogen adsorbed by carbon nanotubes towards the external surface of the sample is accompanied by reversible capture of the diffusant by the chemisorption centres (traps) located on the nanotubes. Within this model, the apparent diffusion coefficient is described by the expression $D_{SWNT} \approx AD_{cap}/K_{(16)I} \approx D_I$ (A = const, D_{cap} is the capillary diffusion coefficient of hydrogen in the absence of chemisorbing traps) similar to Eqn (17).

Taking into account that the experimental values of specific surface area of SWNT samples [76, 204] are typically three – four times smaller than the theoretical value ($S_{sp} \approx 1300$ m^2 g^{-1}),[72] the experimental value x_β should be written in a modified form:

$$x_\beta \approx 2\,\Delta r\, S_{sp}\, \rho\, x_{H_2\beta} \qquad (18a)$$

Substitution of $S_{sp} \approx 400$ (or 1300 m^2 g^{-1}), $x_\beta \approx 0.6 - 1.2$, $\Delta r \approx 0.3$ nm and $\rho \approx 2$ g cm^{-3} (density of the material) [72, 192] into Eqn (18a) gives rise to $x_{H_2\beta} \approx 1.2 - 2.4$ (or 0.4 – 0.8).

For the sorption process corresponding to the peak *I*, Eqns (20) and (21) for $T = 273$ K and $P_{D_2} = 40$ kPa yield $x_{D_2 I} \approx 0.075$, which is substantially smaller than $x_{H_2\beta}$. Thus, it might be assumed that it is physisorption of hydrogen (*i.e.*, condensation of the adsorbate) that dominates in the SWNT samples [18] (peak β) rather than chemisorption as in the case of graphite [181] (peak *I*); to a certain extent, this could be promoted by additional quenching of the SWNT samples at 133 K.

A totally different situation occurs upon hydrogen adsorption on SWNT samples ($x_{SWNT} \approx 0.01$) and graphite powder ($x_{graph} \approx 0.01$) hydrogenated at $T = 295$ K and $P_{H_2} =$ 107 kPa.[85] In a pressure range from 5 kPa to 107 kPa (P_{H_2}), the adsorption process is described by the Henry isotherm, which represents a reduced form of the Henry – Langmuir isotherm [Eqn (20)] at near-zero filling of the sorption centres.

Substitution of the experimental values [85] S_{sp}(SWNT) $\approx$ 504 m^2 g^{-1} and S_{sp}(graph.) $\approx$ 60 m^2 g^{-1} into (18a) yields x_{H_2}(SWNT) ≈ 0.16 and x_{H_2}(graph) ≈ 0.12. Similarly, from Eqns (20) and (21) for $T = 295$ K and $P_{H_2} = 107$ kPa, it follows that $x_{D_2 I} \approx 0.09$, which is close to x_{H_2}(SWNT) and x_{H_2}(graph.). This implies that the mechanism and parameters of hydrogen (deuterium) adsorption by the SWNT and graphite samples [85] studied at a pressure of ~10 – 100 kPa and room temperature are similar to those of the chemisorption process attributed to the peak *I* (Table 3) for isotropic graphite.[181]

The sorption capacity of the graphite sample [85] at 295 K and 107 kPa recalculated for $S_{sp} = 1000$ m^2 g^{-1} is $c_S \approx 1.3$ mass %; the respective sorption capacity of the SWNT samples [85] at the same temperature and hydrogen pressure is $c_S \approx 1.9$ mass %. A similar value $c_S = 1.5 \pm 0.2$ mass % was obtained [72] for electrochemically hydrogenated SWNT and graphite samples with a specific surface area from 50 to 1200 m^2 g^{-1}, which strongly supports the surface character of the sorption processes.

Note that a significantly larger sorption capacity $c_S \approx 10$ mass % – 20 mass % (at 273 K and 40 kPa) was reported for another series of SWNT samples.[18] The reason for this discrepancy is either a strong overestimation of the experimental sorption capacity (by an order of magnitude) or localisation of the dominant fraction of the adsorbate in nanocavities between the tubes, *i.e.*, involvement of the physical mechanism of hydrogen sorption (condensation) under the experimental conditions. (It should also be kept in mind that the SWNT samples [18] were heavily contaminated with soot and subjected to an additional hydrogenation step at 133 K.)

Kinetics of hydrogenation (at $P_{H_2} = 0.1$ MPa and $T = 500$ K) and isothermal hydrogen desorption in a vacuum (at $T = 500$ K) were measured on pads (with a thickness of ~1 mm) composed of tangled bundles of SWNT (50 vol.% – 70 vol.%, diameter of bundles ~15 nm, diameter of nanotubes ~1.4 nm, $S_{sp} \approx 250 - 470$ m^2 g^{-1}, residual content of the catalyst 0.2, 2 and 6%) using the thermo-EMF method.[76] Both processes proceeded as first-order reactions with a relaxation time of $\tau \approx 1$ h. Assuming that the rate-limiting step of the process is diffusion of hydrogen molecules from the surface of the samples to the bulk with the parameters similar to those corresponding to the peak *I* for graphite [181] (Table 3), the estimated length of diffusion path [$L_I \approx (D_I \tau)^{1/2}$] appears similar to the thickness of the pads.

Kinetics of isothermal desorption of hydrogen from electrochemically hydrogenated cylindrical samples ($d = 7$ mm) prepared by cold compacting of a SWNT material (10 mg) mixed with gold powder (90 mg) was studied.[72] Hydrogen content in these SWNT samples reached 0.9 mass %. At 293 K, about half of the total hydrogen amount desorbs during first 10 h whereas the remaining part desorbs for $t_\Sigma \approx 200$ h.[72]

On the basis of diffusion parameters corresponding to the TPD peak *I* for isotropic graphite [181] (Table 3), one can estimate the diffusion coefficient at 293 K to be $D_I = 7.1 \times 10^{-7}$ cm^2 s^{-1}, which is close to $(d^2/t_\Sigma) \approx 6.8 \times 10^{-7}$ cm^2 s^{-1}. This means that it gives a satisfactory description for the process of hydrogen diffusion in such materials.[72]

The same study [72] reported results on hydrogen desorption from SWNT samples hydrogenated at 78 K and 0.2 MPa upon their heating with a rate of $\upsilon \approx 0.067$ K s^{-1} (in a temperature range from 78 K to 800 K) and from graphite samples hydrogenated at room temperature and 2 MPa (for 30 min) upon their cooling to 78 K. For both SWNT and graphite samples, three peaks were revealed [72] at ~105 K, ~136 K and ~300 K. The two latter peaks correspond evidently to peaks α (~150 K) and β (~288 K) observed for the aforementioned SWNT samples studied in Ref. 18. Additional peaks were revealed [72] at ~800 K for the SWNT samples and at ~650 K for the graphite samples,

† In the estimate [18] of sorption capacity of the SWNT samples, a possible involvement of soot and amorphous graphite abundant in the samples (their content reached 99.9 mass % – 99.8 mass %) was not taken into account, peak α was also neglected.

which, probably, can be correlated with peaks *II* and/or *IV* (Fig. 8) for isotropic graphite.[181]

Measurements of hydrogen desorption from samples composed of SWNT bundles, amorphous carbon and particles of a metal catalyst were reported.[34] The samples were first milled in a ball mill (for 24 h in an argon atmosphere) and then exposed to hydrogen for 15 min at $P_{D_2} = 80$ kPa and room temperature. According to electron microscopy,[34] the milling process results in the emergence of deformed areas (defects) in the structure of SWNT bundles and the formation of strongly bent or broken SWNT fibres. TPD curves of the hydrogenated SWNT samples treated in this way (measured at a heating rate of $\upsilon \approx 0.3$ K s^{-1} from $\sim$400 K to $\sim$850 K) reveal a single peak at $\sim$590 K, ($\Delta T \approx 75$ K, $x \approx 0.01$). Based on TPD measurements at different heating rates (from 0.03 to 0.3 K s^{-1}), the activation energy of the process was determined to be $Q_{SWNT} = 145 \pm 20$ kJ mol^{-1}.

The similarity between Q_{SWNT} and Q_{II} implies that the parameters of the diffusion process corresponding to the peak of hydrogen desorption from SWNT bundles[34] are analogous to those of the peak *II* for graphite (Table 3).[181] The length of diffusion path, which characterises the thickness of the samples, estimated from Eqn (2) is L(SWNT) $\approx$ 30 μm.

Within such a model, the apparent diffusion coefficient of hydrogen within the deformed SWNT bundles[34] upon their heating in a vacuum can be described using the following equation: $D_{SWNT} \approx AD_{cap}/K_{(16)II} \approx D_{II}$.

The value $x_{D2II} \approx 0.5$, calculated using Eqns (25) and (26) for 295 K and 80 kPa, can be further used to estimate the atomic (volume) fraction of the deformed areas (η_{II}) within the structure of SWNT bundles. From the expression $x \approx 2\eta_{II} x_{D2II}$, it follows that $\eta_{II} \approx 10^{-2}$. [Most probably, it is the H_2C chemisorption centres of type H (Fig. 9) that are localised in these deformed areas of the SWNT samples.[34]]

Another study[34] was devoted to SWNT, GNF and graphite samples hydrogenated using mechanochemical synthesis in a deuterium atmosphere (in a ball mill at $P_{D_2} =$ 0.9 MPa for 24 h). TPD measurements at a heating rate of $\upsilon \approx 0.08$ K s^{-1} in a temperature range from $\sim$300 K to $\sim$900 K, revealed[34] a peak centred at 740 K (that was distinct in the cases of SWNT and GNF samples but poorly resolved for the graphite samples) and a leading edge of a second peak (especially pronounced for the GNF samples) apparently centred in the range of 900–1100 K. Temperature positions of these peaks are close (taking into account different heating rates υ) to those of peaks α and β observed for the samples of nanostructured graphite[27,29] prepared mechanochemically in a deuterium atmosphere.

It would be useful to consider the experimental results[83] on volume (68 kg m^{-3}) and gravimetric ($x_{exp} \approx 0.48$) hydrogen sorption capacities of SWNT samples (pellets) characterised by S_{sp}(SWNTC) $\approx$ 110 m^2 g^{-1} hydrogenated at $\sim$11 MPa and 295 K. For these conditions, Eqn (18a) gives rise to the value x_{H_2}(SWNT) $\approx$ 3.6 (provided that $S_{sp} = 110$ m^2 g^{-1}) while Eqns (20) and (21)give rise to the value $x_{D_2I} \approx 0.48$, which is close to the ultimate (carbohydride) value (0.5). This discrepancy may be, firstly, due to strongly underestimated experimental specific surface area S_{sp}, which is smaller than the theoretical value by an order of magnitude (see Ref. 72); secondly, it may indicate condensation of the predominant fraction of the adsorbate in the nanocavities between the nanotubes, which is possible at such a high pressure.

Similar values of sorption capacity ($x \approx 0.5$–0.6) were reported in other studies[23,71] for the SWNT samples hydrogenated at 10 MPa and room temperature, which can thus be interpreted analogously.

The interaction of gaseous molecular hydrogen with purified SWNT samples (content of SWNT bundles was $\sim$90 mass %–95 mass %, diameter of the tubes was $\sim$1.38 nm) with the ends open using a chemical treatment with an NaOH aqueous solution was elucidated.[77] The samples with a mass of $\sim$1 g and volume of $\sim$1 cm^3 were hydrogenated at 1.5–9.0 MPa and room temperature ($\sim$295 K). The sorption capacity of the SWNT samples[77] in the case of hydrogenation at 9 MPa and 295 K was x(H/C) = 0.038. The experimental data[77] at $P_{H_2} =$ 1.5–9.0 MPa and $T = 295$ K are described by the Henry adsorption isotherm. TPD measurements with heating rates of $\upsilon = 0.17$ K s^{-1} and 0.017 K s^{-1} revealed peaks centred at $T \approx 508$ K and 374 K, respectively. The enthalpy of activation of the process (Q) determined using the Kissinger procedure was 20 kJ mol^{-1}.

Since the above value of Q coincides with the value of Q_I determined in an analysis of hydrogen desorption from the purified SWNT samples,[77] it is reasonable to utilise the diffusion and sorption parameters corresponding to the peak *I* for graphite (see Table 3).[181] The length of diffusion path calculated using the expression (2) is $L \approx 1$ mm, which corresponds to the thickness of the SWNT samples.[77] Similarly, sorption capacity can be estimated based on Eqns (20) and (21) for 295 K and 9 MPa as $x_{D_2I} \approx 0.47$, which approaches the ultimate (carbohydride) value.

The value x_{H_2}(SWNT) ≈ 0.08 calculated from Eqn (18a) using a typical value of S_{sp}(exp.) = 400 m^2 g^{-1} is substantially smaller than the aforementioned x_{D_2I}. This means that hydrogen sorption on the SWNT samples[77] cannot be described on the basis of the sorption parameters (Table 3) corresponding to the peak *I* for isotropic graphite.[181]

Hydrogen sorption on a new carbon nanomaterial, *viz*., single-walled nanotubes with cone-shaped (horn-like) ends, or nanohorns (SWNH), was studied.[100] The content of SWNH in the samples exceeded 95 mass % while metal catalysts and soot were virtually absent. The original SWNH samples ($S_{sp} \approx 308$ m^2 g^{-1}) and those treated with oxygen at 693 K for 10 min ($S'_{sp} \approx 1006$ m^2 g^{-1}) were tested. Both samples were hydrogenated at $\sim$0.1–6.5 MPa and 303 K. In both cases, the hydrogenation process obeyed the Henry adsorption isotherm (similar to Ref. 77). The sorption capacity of the oxidised samples at 6.5 MPa was $x_{ox} \approx 0.038$ whereas that of the original samples was $x_{init} \approx 0.014$. Substitution of typical experimental values of specific surface area for similar samples into the expression (18a) yields x_{H_2}(ox.) = 0.032 and x_{H_2}(init.) = 0.038. On the other hand, the value calculated using Eqns (20) and (21) for 303 K and 6.5 MPa, $x_{D_2I} = 0.46$ [which is close to the ultimate (carbohydride) value of 0.5], is larger than the above x_{H_2}(ox.) and x_{H_2}(init.) values by an order of magnitude.

These results are similar to those obtained in the above analysis of the experimental data from Ref. 77 but drastically different from those of Ref. 83. The latter results were obtained at a similarly high pressure for the SWNT samples that have not been purified from soot, amorphous carbon and particles of metal catalysts. Therefore, the presence of soot, amorphous carbon and metal catalyst in the SWNT samples strongly affects the overall sorption process.

8. Sorption and diffusion of hydrogen in multi-walled carbon nanotubes

Sorption of hydrogen by two types of MWNT samples (with a mass of $\sim$2 mg) having different structures were studied by Lee *et al*.[89] The samples were exposed to hydrogen for 5 h at 4 MPa and 300 K (with subsequent cooling down to 80 K) and then studied using TPD (at $\upsilon = 0.03$–0.08 K s^{-1}).

The first type (A) of the samples were composed of strongly bent nanotubes with strongly distorted graphene layers and partially blocked nanoholes. Side faces of the majority of the tubes were closed. External and internal diameters of the tubes were estimated[89] to be 10–30 nm and 5–15 nm, respectively, and the specific area amounted to S_{sp}(A) $\approx$ 174 m^2 g^{-1}. The samples A manifested two TPD peaks: a peak α_1 around 312 K ($\Delta T_{\alpha 1} \approx 18$ K, $\upsilon = 0.05$ K s^{-1}, $Q_{\alpha 1} \approx 18.5$ kJ mol^{-1}, $x_{\alpha 1} \approx 7.7 \times 10^{-2}$) and a peak β_1 around 419 K ($\Delta T_{\beta_1} \approx 8$ K, $\upsilon = 0.05$ K c^{-1}, $Q_{\beta 1} \approx 124.4$ kJ mol^{-1}, $x_{\beta 1} \approx 3.6 \times 10^{-3}$). The peak α_1 reappeared upon several consecutive cycles of hydro-

genation and heating of the samples whereas the peak β_1 did not reappear.

The samples B were composed of straightened, aligned MWNT with a less distorted structure as compared to the samples A. Nanoholes within the samples B were assembled into pores and side faces of the tubes remained open. The external and internal diameters of the tubes were $\sim$20 nm and $\sim$8 nm, respectively; specific surface area $S_{sp}(B) \approx 877$ m^2 g^{-1} [this value is several times larger than the theoretical value of the specific surface area (263 m^2 g^{-1}) [72] for ten-walled nanotubes]. The samples B manifested only one TPD peak (α_2) around 313 K ($\Delta T_{\alpha 2} \approx 7$ K, $\upsilon = 0.05$ K c^{-1}, $Q_{\alpha 2} \approx 16.5$ kJ mol^{-1}, $x_{\alpha 2} \approx 0.24$).[89]

The similarity between $Q_{\alpha 1}$ and $Q_{\alpha 2}$, on the one hand, and Q_I in graphite,[181] on the other hand, indicates that the parameters characterising the TPD peak *I* (Table 3) for isotropic graphite [181] can be used to describe peaks α_1 and α_2 for the MWNT samples.[89] The lengths of diffusion path $L_{\alpha 1}$ and $L_{\alpha 2}$, which characterise thickness of the samples, calculated on the basis of Eqn (2) are 130–200 μm.

The ratio $x_{\alpha 2}/x_{\alpha 1}$ is close to the ratio $S_{sp}(A)/S_{sp}(B)$, which is in agreement with the published results.[72, 81] The local concentration of hydrogen molecules within the adsorbed layers on the walls of the nanotubes calculated using Eqn (18a) is $\sim$0.2–0.3. For the experimental conditions used in Ref. 89, Eqns (20) and (21) yield $x_{D_2 I} \approx 0.4$. This value of $x_{D_2 I}$ is close to $x_{H_2 \alpha}$ calculated from the experimental data [*i.e.*, $x_{\alpha 1}$, $S_{sp}(A)$, $x_{\alpha 2}$, $S_{sp}(B)$] for the MWNT samples.[89]

The similarity between $Q_{\beta 1}$ and Q_{II} assumes that the peak β_1 for the samples A is analogous (with regard to diffusion parameters) to the peak *II* (Table 3) for isotropic graphite.[181] The absence of the peak β_1 in subsequent cycles of hydrogenation and annealing of the samples A [89] can be explained by curing of the deformational structural defects in these samples upon their first annealing. The length $L_{\beta 1} \approx 0.2$ μm calculated using Eqn (2) probably characterises the diffusion dimension of the distorted areas within the samples A.[89] The volume fraction of such distorted areas within the samples A with chemisorbing carbon 'centres' can be estimated using the equation $x_{\beta 1} = 2\eta_{\beta 1} x_{D_2 II}$, where $x_{D_2 II} \approx 0.5$ [as determined from the expressions (25) and (26)] to $\eta_{\beta 1} \approx 4 \times 10^{-3}$.

Sorption of hydrogen by MWNT samples at 10 MPa and room temperature was studied by Li *et al.*[90] They used two types of samples: one type of the samples (A) was characterised by numerous cracks in the external graphene layers (walls) of nanotubes even after annealing at 2473 K (for 2 h); another type (B) was characterised by crack-less graphene layers (walls) both before and after annealing at 2473 K (for 2 h). Sorption capacities (x) of the non-annealed samples A and B were 0.1 and 0.09, respectively whereas those of the annealed samples were 0.5 and 0.1, respectively.

Specific surface areas of the samples A and B [90] calculated using Eqns (18a), (20) and (21) are $\sim$520 m^2 g^{-1} and $\sim$110 m^2 g^{-1}, respectively. These calculated values of S_{sp} are within the range of typical values found experimentally for such materials, which implies that the process of hydrogen sorption on the MWNT samples [90] can be described using the parameters corresponding to the peak *I* for graphite.[181]

Sorption of hydrogen by MWNT samples with a diameter of 10–40 nm (predominantly with closed side faces) at 290 K and $P_{H_2} = 3$–10 MPa was studied by Cao *et al.*[91] They used two types of samples: samples A composed of straightened highly oriented nanotubes [tube density was up to $\sim 10^8$ mm^{-2}, thickness of some tube blocks was $h \approx 250$ μm, $S_{sp}(A) \approx 60$ m^2 g^{-1}] and samples B characterised by a random arrangement of the nanotubes [and variable nanoporosity, $S_{sp}(B) \approx 27$ m^2 g^{-1}].

For both types of the MWNT samples (A and B), the hydrogen uptake increased linearly with an increase in pressure P_{H_2} from 3 to 10 MPa.[91] Sorption capacities (x) of the samples A and B at 290 K and 10 MPa were $\sim$0.29 and $\sim$0.082, respectively. Hydrogenation of the samples A resulted in disappearance of pores in the size range of 10–100 nm and an increase in the number of pores in the size range of 2–10 nm, which can be due to development of local strains and deformations.[154, 184–187]

Sorption capacity x_{H_2}, determined using the expression (18a) and experimental values of $x(A)$, $x(B)$, $S_{sp}(A)$ and $S_{sp}(B)$ is 2.2–3.6, which is significantly larger than $x_{D_2 I} \approx 0.46$, estimated on the basis of Eqns (20) and (21) for 290 K and 10 MPa. Presumably, this discrepancy is due to inaccurate determination of the specific surface areas of the MWNT samples [91] (the experimental values of S_{sp} were measured using the BET adsorption isotherms of nitrogen rather than hydrogen at 77 K and thus were underestimated). The high values of x_{H_2} can be also explained by condensation of a large fraction of the adsorbate in the nanocavities between the tubes of the MWNT samples,[91] *i.e.*, domination of physisorption over chemisorption with the parameters corresponding to the peak *I* for graphite.[181]

Characteristics of hydrogen sorption on straightened (aligned) multi-walled nanotubes with a diameter of 50–100 nm and density of $\sim 10^8$–10^9 mm^{-2} were reported by Chen *et al.*[88] The samples were hydrogenated at $\sim$295 K and $\sim$0.1 MPa (or $\sim$1.0 MPa) up to hydrogen concentration $x_{exp} \approx 0.60$–0.84 (or 1.08–1.56), then treated with nitric acid and annealed at 673 K.

Upon heating of the hydrogenated samples (with a mass of $\sim$1 mg) from $\sim$295 K to 573 K with a rate of $\upsilon \approx 0.083$ K s^{-1}, several hydrogen desorption peaks were detected by mass spectrometry.[88] The major peak (about 90%) was centred at $T \approx 540$ K with a width at half maximum of $\Delta T \approx 45$ K, *i.e.*, the dominant fraction of adsorbed hydrogen was liberated from the MWNT samples at 500–600 K.[88]

The length of diffusion path of hydrogen estimated using Eqn (2) is $L \approx 15$ μm. This value is comparable with the mean length of the nanotubes and thickness of the MWNT samples.[88] This indicates that the diffusion process corresponding to the peak at 540 K for the MWNT samples [88] is characterised by parameters similar to those attributed to the peak *II* for graphite.[181]

Substitution of $x_{D_2 II} \approx 0.5$ calculated using Eqns (25) and (26) and the experimental value $0.9\,x_{exp} \approx 0.54$–0.76 into Eqn (18a) gives rise to $S_{sp} \approx 500$–700 m^2 g^{-1}, which is significantly larger than the ultimate theoretical value.[72] Therefore, it might be assumed that in this case, the dominant part of the adsorbate undergoes condensation in the nanocavities between the tubes of the MWNT samples.[88]

Chen et al. [88] noted that the cone-shaped structure of studied samples was different from that typical of ideal MWNT samples and rather similar to GNF samples.[32, 33, 205]

9. An analysis of abnormal data concerning hydrogen sorption by graphite nanofibres

In 1998, Chambers *et al.* published a sensational paper [33] on the possibility of hydrogen storage in a new materials, *viz.*, graphite nanofibres‡ with a specific structure. They reported that GNF samples with an oriented (at $\sim$45°) nanostructure are capable of sorbing an abnormally high amount of hydrogen ($x_\Sigma \approx 18.5$) at $P_{H_2} \approx 9.6$ MPa (final value) and $T = 298$ K.

Hydrogenation of the GNF samples lasted for 20 h (τ_Σ). Upon release of the pressure, the dominant fraction of adsorbed hydrogen ($x \approx 9.8$) desorbed during $\tau \approx 5$–10 min.

Chambers *et al.* [33] also hydrogenated a series of other materials, including palladium powder (up to final composition of $PdH_{2.2}$, which differs from the stoichiometry of stable Pd_2H and metastable $PdH_{1.1-1.3}$ palladium hidrides [177]) and $LaNi_5$. The sorption capacities of these materials were overestimated as well,

‡ The nanofibres with a length of $\sim$10–100 μm were composed of stacks of strictly oriented (parallel, perpendicular, or at an angle of $\sim$45° with respect to the stack axis) graphene platelets with a distance between the graphene sheets of $\geqslant$0.335 nm (which is close to the interlayer separation in graphite [181]) and a cross-section area of $\sim$0.3–5.0 nm^2. This material represented a system of spot-like nanopores with open ends.[33]

which, according to Nishimiya *et al.*,[85] can be considered as additional evidence for a systematic error in the measurements of hydrogen sorption by GNF performed by Chambers *et al.*[33] Results regarding hydrogenation of graphite (at $\sim$11 MPa and 298 K for $\sim$40 h) up to a concentration of $x_\Sigma \approx 0.57$ and activated carbon 'Norite' characterised by $S_{sp} \approx 1000$ m^2 g^{-1} up to a concentration of $x_\Sigma \approx 0.20$ were also significantly different from those reported by other groups.[35, 38, 72, 85, 141]

In a subsequent study of hydrogen sorption by GNF samples, the same group of authors [32] reported much lower values $x_\Sigma \approx 8.0$ (hydrogenation was performed at $P_{H_2} \approx 11.2$ MPa and 298 K for 24 h).§ Furthermore, the authors noted that achievement of such a high value of x_Σ required an additional short *in situ* annealing of the GNF samples at 473 K.

Followed by release of the high pressure and retention of the hydrogenated samples at 298 K for $\tau_\alpha \geqslant 10$ min giving rise to desorption of the dominant fraction of hydrogen ($x_\alpha \approx 5.9$, peak α), the GNF samples were heated again to $\sim$1223 K at a rate of $\upsilon \approx 0.17$ K s^{-1}. Upon this second heating, the TPD curve (Fig. 13) revealed two peaks (β and γ) centred at 880 K ($\Delta T_\beta \approx 245$ K, $x_\beta \approx 1.2$) and 1140 K ($\Delta T_\gamma \approx 205$ K, $x_\gamma \approx 0.9$). Around T_β, a concomitant liberation of gaseous hydrocarbons (CH_4, *etc.*) was detected.

A comparison of the TPD curves (Fig. 13) for the GNF samples hydrogenated at 11 MPa (curve *1*) and 0.1 MPa (curve *2*) shows that the sorption process corresponding to the peak β is described by the Henry – Langmuir adsorption isotherm and that corresponding to the peak γ is described by the Sieverts – Langmuir isotherm. The peak β is analogous to the peak *II* in the case of isotropic graphite,[181] whereas the peak γ is analogous to the peak *III*. Therefore, in order to calculate the respective length of diffusion path of hydrogen in the GNF samples (for peak β), one can utilise Eqn (2). The value $L_\beta \approx 0.4$ cm determined in this way corresponds to the linear size of the GNF sample ($l \approx 0.6 - 0.8$ cm).[32]

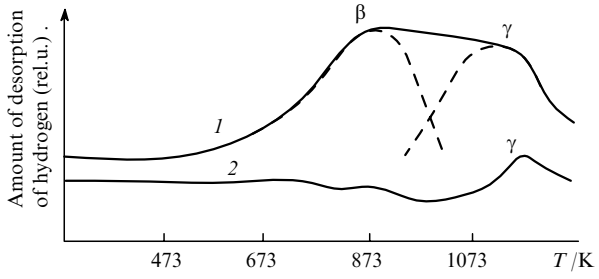


Figure 13. Temperature-programmed desorption of hydrogen from the GNF samples hydrogenated at 11.2 MPa (*1*) and 0.1 MPa (*2*) (for assignment of the TPD peaks, see text).
The experimental curves are shown as solid lines, individual components of the curve (*1*) are shown as dotted lines.

The value of sorption capacity $x_{H_{2\beta}}$ calculated using the equation $x_\beta \approx 12\,(\Delta r/d_{GNF})x_{H_2\beta}$ ($\Delta r \approx 0.2$ nm, $d_{GNF} \approx 1$ nm)[32] is $\sim$0.5. A similar value is obtained for x_{D_2II} on the basis of Eqns (25) and (26).

The experimental value x_γ is in fair agreement with the value $x_{III} \approx 0.6$ calculated using Eqns (9) and (10) for the peak *III* (Table 3). Also note that the values of x_γ, x_{III}, $x_{H_2\beta}$ and x_{D_2II} are close to the ultimate (carbohydride) values of $(x_{III})_{max}$ and $(x_{II})_{max}$.

The length of diffusion path ($L_\gamma \approx 50$ nm) estimated on the basis of parameters of the peak γ (for the GNF samples) according to Eqn (3) using D_{III} (Table 3) is significantly larger than $d_{GNF} \approx 1$ nm.[32, 33] There are two possible reasons for the difference between L_γ and d_{GNF}: either the value of diffusion coefficient used in the calculation of L_γ is overestimated ¶ or the value of d_{GNF} as determined in Ref. 32 is incorrect.† This can be due to the formation of a specific substructure (with a characteristic linear size of $\sim$1 – 3 nm) in the hydrogenated GNF samples [32] (having a fibre diameter of $\sim$50 nm), which disappears (due to curing) upon heating of the samples in the course of the TPD measurements. This suggestion is supported by the results of other studies,[32, 91] which revealed an abrupt decrease in the hydrogen concentration and a change in the size of nanopores within the hydrogenated GNF and MWNT samples and their reappearance upon heating.

It should be emphasised that the parameters of sorption and diffusion processes corresponding to peaks β and γ for the GNF samples [32] agree with those of processes corresponding to peaks α and β for nanocrystalline graphite [29] and are satisfactorily described by the parameters of peaks *II* and *III* for isotropic graphite (Table 3).[181]

The apparent diffusion coefficient of hydrogen in the GNF samples,[32] which characterises the process of desorption of the dominant fraction (x_α) of hydrogen at 298 K (peak α that appears just after release of the high pressure), can be estimated as $D_\alpha \approx (L^2/\tau_\alpha) \approx 2 \times 10^{-3}$ cm^2 s^{-1}. This value is larger by 3.5 orders of magnitude than D_I (peak *I*, Table 3) typical of graphite.[181] This strongly assumes different mechanisms of hydrogen sorption on GNF [32] and graphite [181] around T_α and T_I.

The sorption capacity corresponding to the peak α cannot be described using the parameters attributed to the peak *I* for isotropic graphite.[181] Thus, there are serious reasons validating the suggestion [32, 33] that the desorption process corresponding to the peak α is essentially due to the removal of hydrogen condensate from the nanocavities of the graphite nanofibres. Additionally, this is supported by the neutron diffraction data [4, 32] on abnormally high packing density (which exceeds that of hydrogen molecular crystals) of the adsorbate on the graphite surface and X-ray diffraction data [26] on an abnormally large increase (by 40%) in the interplane separation observed for the GNF samples hydrogenated at 9 GPa.

V. Conclusion

The comparative and constructive thermodynamic analyses of the experimental and theoretical data on the sorption of hydrogen by carbon nanomaterials in technically reasonable ranges of pressure and temperature confirm that the abnormally large scatter (up to three orders of magnitude) and poor reproducibility (or even lack of reproducibility) of the measurements of sorption capacities of these materials is caused by a number of factors, including complexity of the objects under study, variations in the microstructure (that strongly depends upon method used for the preparation of the sorbents) and conditions of physicochemical pretreatment and modes of hydrogenation of the samples, etc. The state-of-the-art in investigations into the interactions of hydrogen with graphite and carbon nanomaterials makes it possible to deliberately optimise synthetic conditions and modes of hydrogenation for such materials, which is an absolute prerequisuite for advancement towards creation of superadsorbents for hydrogen.

The authors are grateful to their colleagues, A K Chernysheva and E V Borisov, for the fruitful discussion of the results.

§ These data were neither confirmed by other researchers.

¶ It might be assumed that the diffusion coefficient of hydrogen atoms in the 'hydrocarbon phase' of GNF is smaller than that in the graphite lattice [181] with partially occupied carbon chemisorption centres, therefore, the value of D_{III} should not be used in a calculation of L_γ.

† There is experimental evidence [35, 71, 141, 142, 206] that the graphite nanofibres were characterised by a larger diameter ($d_{GNF} \approx 10 - 100$ nm) than that reported in Ref. 32.

References

1. D Yu Gamburg, M F Dubovkin *Vodorod. Svoistva, Poluchenie, Khranenie, Transportirovanie, Primenenie. Spravochnoe Izdanie* (Hydrogen. Properties, Production, Storage, Transport, Applications. Handbook) (Moscow: Khimiya, 1989)
2. P M Grant *Nature* (*London*) **424** 129 (2003)
3. *Poisk* (3) (765) 15 (2004); http://www.poisknews.ru/-ingz/arkiv.asp
4. A C Dillon, M J Heben *Appl. Phys. A* **72** 133 (2001)
5. L Schlapbach, A Züttel *Nature* (*London*) **414** 353 (2001)
6. S Hynek, W Fuller, J Bentley *Int. J. Hydrogen Energy* **22** 601 (1997)
7. M Junker, L Bocquet, M Bendif, D Karboviac *Ann. Chim. Sci. Mat.* **26** 117 (2001)
8. M Schrope *Nature* (*London*) **414** 682 (2001)
9. R Chahine, T K Bose *Int. J. Hydrogen Energy* **19** 161 (1994)
10. E Poirier, R Chahine, P Bénard, D Cossement, L Lafi, E Mélancon, T K Bose, S Désilets *Appl. Phys. A* **78** 961 (2004)
11. S Iijima *Nature* (*London*) **354** 56 (1991)
12. A V Eletskii, B M Smirnov *Usp. Fiz. Nauk* **163** 33 (1993) [a]
13. M Inagaki, L R Radovic *Carbon* **40** 2279 (2002)
14. B P Tarasov, N F Goldshdeger, A P Moravsky *Usp. Khim.* **70** 149 (2001) [*Russ. Chem. Rev.* **70** 131 (2001)]
15. A L Ivanovskii *Usp. Khim.* **68** 119 (1999) [*Russ. Chem. Rev.* **68** 103 (1999)]
16. A L Ivanovskii *Usp. Khim.* **71** 203 (2002) [*Russ. Chem. Rev.* **71** 175 (2002)]
17. B M Smirnov *Khimiya Nanostruktur. Sintez, Stroenie, Svoistva* (The Chemistry of Nanostructures. Synthesis, Structure, Properties) (St Petersburg: St Petersburg State University, 1996)
18. A C Dillon, K M Jones, T A Bekkedahl, C H Kiang, D S Bethune, M J Heben *Nature* (*London*) **386** 377 (1997)
19. I O Bashkin, in *International Symposium on Metal Hydrogen Systems (Abstracts of Reports), Annecy, France, 2002* p. 28
20. D J Browning, M L Gerrard, J B Laakeman, I M Mellor, R J Mortimer, M C Turpin, in *Proceedings of the 13th World Hydrogen Energy Conference, Beijing, China, 2000* p. 580
21. X D Bai, D Zhong, G Y Zhang, X C Ma, S Liu, E G Wang, Y Chen, D T Shaw *Appl. Phys. Lett.* **79** 1552 (2001)
22. M Hirscher, M Becher, M Halushka, F Zeppelin, X Chen, U Dettlaff-Weglikowska, S Roth *J. Alloys Compd.* **356-357** 433 (2003)
23. H W Zhu, A Chen, Z Q Mao, C L Xu, X Xiao, B Q Wei, J Liang, D H Wu *J. Mater. Sci. Lett.* **19** 1237 (2000)
24. H M Cheng, C Liu, Y Y Fan, F Li, G Su, L L He, M Liu *Z. Metallkd.* **91** 306 (2000)
25. A C Dillon, P A Parilla, K M Jones, G Riker, M J Heben, in *Proceedings of the 1998 U.S.DOE Hydrogen Program Review*. NREL/CP-570-25315
26. I O Bashkin, V E Antonov, A V Bazhenov, I K Bdikin, D N Borisenko, E P Krinichnaya, A P Moravskii, A I Kharkunov, Yu M Shul'ga, Yu A Osip'yan, E G Ponyatovskii *Pisma Zh. Eksp. Teor. Fis.* **79** 280 (2004) [b]
27. S Orimo, G Majer, T Fukunaga, A Züttel, L Schlapbach, H Fujii *Appl. Phys. Lett.* **75** 3093 (1999)
28. G Majer, U Eberle, F Kimmerle, E Stanik, S Orimo *Physica B* **328** 81 (2003)
29. S Orimo, T Matsushima, H Fujii, T Fukunaga, G Majer *J. Appl. Phys.* **90** 1545 (2001)
30. T Fukunaga, K Itoh, S Orimo, M Aoki, H Fujii *J. Alloys Compd.* **327** 224 (2001)
31. H Fujii, S-i Orimo *Physica B* **328** 77 (2003)
32. C Park, P E Anderson, A Chambers, C D Tan, R Hidalgo, N M Rodrigues *J. Phys. Chem. B* **103** 10572 (1999)
33. A Chambers, C Park, R T K Baker, N M Rodriguez *J. Phys. Chem. B* **102** 4253 (1998)
34. M Hirscher, M Becher, M Galuska, A Quintel, V Skakalova, Y-M Choi, U Dettlaff-Weglikowska, S Roth, I Stepanek, P Bernier, A Leonhardt, J Fink *J. Alloys Compd.* **330-332** 654 (2002)
35. C C Ahn, Y Ye, B V Ratnakumar, C Witham, R C Bowman Jr, B Fultz *Appl. Phys. Lett.* **73** 3378 (1998)
36. J Y Hwang, S H Lee, K S Sim, J W Kim *Synth. Met.* **126** 81 (2002)
37. M Ritschell, M Uhlemann, O Gutfleish, A Leonhardt, A Graff, Ch Tuschner *Appl. Phys. Lett.* **80** 2985 (2002)
38. G G Tibbetts, G P Meisner, Ch H Olk *Carbon* **39** 2291 (2001)
39. R T Yang *Carbon* **38** 623 (2000)
40. P Chen, X Wu, J Lin, K L Tan *Science* **285** 91 (1999)
41. O K Alexeeva, in *Proceedings of the VIIth International Conference 'Hydrogen Materials Science'* (Kiev: ADEF-Ukraine, 2001) p. 672
42. Yu S Nechaev, D V Iourtchenko, T N Veziroglu, in *Proceedings of the International Conference of American Carbon Society 'Carbon 2004', Providence, RI, 2004* p. 250
43. Yu S Nechaev, O K Alekseeva, in *Materialy Nauchno-Prakticheskoi Konferentsii Materialovedcheskikh Obshchestv Rossii 'Novye Funktsional'nye Materialy i Ekologiya', Moskva, 2002* (Proceedings of the Scientific and Practical Conference of Materials Science Societies 'New Functional Materials and Ecology', Moscow, 2002) p. 75
44. Yu S Nechaev, D V Iourtchenko, T N Veziroglu, in *Proceedings of the 15th World Hydrogen Energy Conference, Yokohama, Japan, 2004* p. 310
45. Yu S Nechaev, D V Iourtchenko, T N Veziroglu, in *Proceedings of the VIIIth World Renewable Energy Congress, Denver, CO, 2004* p. 270
46. Yu S Nechaev, O K Alekseeva, in *Sbornik Tezisov Dokladov II Mezhdunarodnogo Simpoziuma 'Bezopasnost' i Ekonomika Vodorodnogo Transporta', Sarov, 2003* (Abstracts of Reports of the IIth International Symposium 'Safety and Economics of Hydrogen Transport', Sarov, 2003) p. 138
47. Yu S Nechaev, O K Alekseeva, in *Sbornik Rasshirennykh Tezisov Dokladov VIII Mezhdunarodnoi Konferentsii 'Vodorodnoe Materialovedenie i Khimiya Uglerodnykh Nanomaterialov' (ICHMS'2003), Sudak, 2003* [Expanded Abstracts of the VIIIth International Conference 'Hydrogen Materials Science and Chemistry of Carbon Nanostructures (ICHMS'2003)', Sudak, Ukraine, 2003] p. 774
48. Yu S Nechaev, O K Alexeeva, J G Hirschberg, T N Veziroglu, in *The Vth International Conference 'Hydrogen Power Theoretical and Engineering' (Abstracts of Reports), Porto Conte, 2003* p. 97
49. M Hirscher, M Becher, M Haluska, X Chen, U Dettlaff-Weglikowska, S Roth, in *International Symposium on Metal Hydrogen Systems (Abstracts of Reports), Annecy, France, 2002* p. 29
50. S Orimo, T Matsushima, P Wang, H Fujii, T Fukunaga, G Majer, A Züttel, L Schlapbach, in *International Symposium on Metal Hydrogen Systems (Abstracts of Reports), Annecy, France, 2002* p. 28
51. B P Tarasov, in *Sbornik Tezisov Dokladov II Mezhdunarodnogo Simpoziuma 'Bezopasnost' i Ekonomika Vodorodnogo Transporta', Sarov, 2003* (Abstracts of Reports of the IIth International Symposium 'Safety and Economics of Hydrogen Transport', Sarov, 2003) p. 38
52. B P Tarasov, N F Goldshleger *Al'ternat. Energ. Ekol.* **3** 20 (2001)
53. D V Schur, B P Tarasov, Y M Shul'ga, S Yu Zaginaichenko, Z A Matysina, A P Pomytkin *Carbon* **41** 1331 (2003)
54. H-M Cheng, Q-H Yang, C Liu *Carbon* **39** 1447 (2001)
55. Z Liu, X-H Chen, H-H Song *New Carbon Mater.* **17** 73 (2002)
56. F Darkrim, P Malbrunot, G P Tartaglia *Int. J. Hydrogen Energy* **27** 193 (2002)
57. V V Simonyan, J K Johnson *J. Alloys Compd.* **330-332** 659 (2002)
58. E G Rakov *Usp. Khim.* **70** 934 (2001) [*Russ. Chem. Rev.* **70** 827 (2001)]
59. S Orimo, A Züttel, L Schlapbach, G Majer, T Fukunaga, H Fujii *J. Alloys Compd.* **356-357** 716 (2003)
60. J Conard *Ann. Chim. Sci. Mat.* **26** 107 (2001)
61. M S Dresselhaus, K A Williams, P C Eklund *MRS Bull.* **24** 145 (1999)
62. Z-Q Yang, Z-L Xie, Y-S He *New Carbon Mater.* **18** 75 (2003)
63. Yu S Nechaev, O K Alexeeva *Int. J. Hydrogen Energy* **28** 1433 (2003)

64. A Badzian, T Badzian, E Breval, A Piotrowski *Thin Solid Films* **398-399** 170 (2001)
65. L Schlapbach, A Züttel, P Grlning, O Gröning, P Aebi *Appl. Phys. A* **72** 245 (2001)
66. P Bénard, R Chahine *Langmuir* **17** 1950 (2001)
67. E A Evard, A P Voit, S K Gordeev, I E Gabis *Fiz.-Khim. Mekh. Mater.* **36** 23 (2000)
68. E A Denisov, T N Kompaniets, I V Makarenko, Z Vakar, A N Titkov *Materialovedenie* (2) 45 (2002)
69. E A Denisov, T N Kompaniets, A A Kurdyumov *NATO Sci. Ser. II, Math., Phys., Chem.* **1** 273 (2000)
70. Y Ye, C C Ahn, C Witham, B Fultz, J Liu, A G Rinzier, D Colbert, K A Smith, R E Smalley *Appl. Phys. Lett.* **74** 2307 (1999)
71. C Liu, Y Y Fan, M Liu, H T Cong, M S Dresselhaus *Science* **286** 1127 (1999)
72. A Züttel, P Sudan, Ph Mauron, Ph Mauron, T Kiyobaushi, Ch Emmenegger, L Schlapbach *Int. J. Hydrogen Energy* **27** 203 (2002)
73. A C Dillon, K E H Gilbert, P A Parilla, J L Alleman, G L Hornyak, K M Jones, M J Heben, in *Proceedings of the 2002 U.S. DOE Hydrogen Program Review NREL/CP-610-32405, Golden, CO, 2002*
74. M Shiraishi, T Takenobu, A Yamada, M Ata, H Kataura *Chem. Phys. Lett.* **358** 213 (2002)
75. T Takenobu, M Shiraishi, A Yamada, M Ata, H Kataura, Y Iwasa *Synth. Met.* **135-136** 787 (2003)
76. B K Pradhan, G U Sumanasekera, K W Adu, H E Romero, K A Williams, P C Eklund *Physica B* **323** 115 (2002)
77. M Shiraishi, T Takenobu, M Ata *Chem. Phys. Lett.* **367** 633 (2003)
78. H W Zhu, A Y Cao, X S Li , C L Xu, Z Q Mao, D B Ruan, J Liang, D H Wu *Appl. Surf. Sci.* **178** 50 (2001)
79. L Ci, H Zhu, B Wei, C Hu, D Wu *Appl. Surf. Sci.* **205** 39 (2003)
80. B Renker, H Schober, P Schweiss, S Lebedkin, F Henrich *Condens. Mater.* **1** 1266 (2003)
81. B P Tarasov, J P Maehlen, M V Lototsky, V E Muradyan, V A Yartys *J. Alloys Compd.* **356-357** 510 (2003)
82. H Kajiura, S Tsutsui, K Kadono, M Kakuta, M Ata, Y Murakami *Appl. Phys. Lett.* **82** 1105 (2003)
83. C Liu, Q H Yang, Y Tong, H T Cong, H M Cheng *Appl. Phys. Lett.* **80** 2389 (2002)
84. M R Smith Jr, E W Bittner, W Shi, J K Johnson, B C Bockrath *J. Phys. Chem. B* **107** 3752 (2003)
85. N Nishimiya, K Ishigaki, H Takikawa, M Ikeda, Y Hibi, T Sakakibara, A Matsumoto, K Tsutsumi *J. Alloys Compd.* **339** 275 (2002)
86. M M Shaijumon, S Ramaprabhu *Chem. Phys. Lett.* **374** 513 (2003)
87. R Zidan, A M Rao, in *Proceedings of the 2002 U.S. DOE Hydrogen Program Review NREL/CP-610-32405, Golden, CO, 2002*
88. Y Chen, D T Shaw, X D Bai, E J Wang, C Lund, W M Lu, D D L Chung *Appl. Phys. Lett.* **78** 2128 (2001)
89. H Lee, Y-S Kang, S-H Kim, J-Y Lee *Appl. Phys. Lett.* **80** 577 (2002)
90. X Li, H Zhu, L Ci, C Xu, Z Mao, B Wei, J Liang, D Wu *Carbon* **39** 2077 (2001)
91. A Cao, H Zhu, X Zhang, X Li, D Ruan, C Xu, B Wei, J Liang, D Wu *Chem. Phys. Lett.* **342** 510 (2001)
92. H Gao, X B Wu, J T Li, G T Wu, J Y Lin, K Wu, D S Xu *Appl. Phys. Lett.* **83** 3389 (2003)
93. C Park, C D Tan, R Hidalgo, A Chambers, R T K Baker, N M Rodriguez, in *Proceedings of the 1998 U.S. DOE Hydrogen Program Review NREL/CP-570-25315*
94. M Rzepka, P Lamp, M A de la Casa-Lillo *J. Phys. Chem. B* **102** 10894 (1998)
95. B K Gupta, O N Srivastava *Int. J. Hydrogen Energy* **25** 825 (2000)
96. B K Gupta, O N Srivastava *Int. J. Hydrogen Energy* **26** 857 (2001)
97. B K Gupta, in *Extended Abstracts of the VIIIth International Conference 'Hydrogen Materials Science and Chemistry of Carbon Nanostructures (ICHMS'2003)', Sudak, Ukraine, 2003* p. 794
98. K Hanada, H Shiono, K Matsuzaki *Diamond Relat. Mater.* **12** 874 (2003)
99. K Kadono, H Kajiura, M Shiraishi *Appl. Phys. Lett.* **83** 3392 (2003)
100. K Murata, K Kaneko, H Kanoh, D Kasuya, K Takahashi, F Kokai, M Yudasaka, S Iijima *J. Phys. Chem. B* **106** 11132 (2002)
101. E Johansson, B Hjorvarsson, T Ekstrom, M Jacob *J. Alloys Compd.* **330-332** 670 (2002)
102. H Kajiura, K Kadono, S Tsutsui, Y Murakami *Appl. Phys. Lett.* **82** 1929 (2003)
103. J C Wang, R W Murphy, F C Ten, R O Loutfy, E Veksler, W Li, in *Proceedings of the 1998 U.S.DOE Hydrogen Program Review NREL/CP-570-25315*
104. C Lenardi, E Barborini, V Briois, L Lucarelli, P Piseri, P Milani *Diamond Relat. Mater.* **10** 1195 (2001)
105. P Milani, P Piseri, E Barborini, C Lenardi, M Marino, S Maffi, V Briois, in *Proceedings of the VIIth International Conference 'Hydrogen Materials Science'* (Kiev: ADEF-Ukraine, 2001) p. 502
106. H Takagi, H Hatori, Y Soneda, Y Yamada *TANSO* (205) 231 (2002)
107. D Lupu, A R Biris, I Misan, A Jianu, G Holzhuter, E Burkel *Int. J. Hydrogen Energy* **29** 97 (2004)
108. W Muller *J. Nucl. Mater.* **162-164** 138 (1989)
109. R A Causey *J. Nucl. Mater.* **162-164** 151 (1989)
110. D S Rawat, S Talapatra, K Lafdi, A D Migone *Appl. Phys. A* **78** 969 (2004)
111. W-Q Deng, X Xu, W Goddard *Phys. Rev. Lett.* **92** 166103 (2004)
112. A Züttel, Ch Nutzenadel, P Sudan, Ph Mauron, Ch Emmenegger, S Rentsch, L Schlapbach, A Weidenkaff, T Kiyobayashi *J. Alloys Compd.* **330-332** 676 (2002)
113. G-P Dai, M Liu, M-Z Wang, H-M Cheng *New Carbon Mater.* **17** 70 (2002)
114. X Yan, X Gao, Y Li, Z Liu, F Wu, Y Shen, D Song *Chem. Phys. Lett.* **372** 336 (2003)
115. M Miranda-Hernández, J-A Ayala, M E Rincón *J. Solid State Electrochem.* **7** 264 (2003)
116. D Hao, H Zhu, X Zhang, Y Li, C Xu, Z Mao, J Liu, D Wu *Chin. Sci. Bull.* **48** 538 (2003)
117. C Nutzenadel, A Züttel, D Chartouni, L Schlapbach *Electrochem. Solid-State Lett.* **2** 30 (1999)
118. G-P Dai, M Liu, D M Chen, P X Hou, Y Tong, H-M Cheng *Electrochem. Solid-State Lett.* **5** E13 (2002)
119. E Frackowiak, F Béguin *Carbon* **40** 1775 (2002)
120. K Jurewicz, E Frackowiak, F Béguin *Appl. Phys. A* **78** 981 (2004)
121. L Lombardi, M Bestetti, C Mazzocchia, P L Cavalotti, U Ducati *Electrochem. Solid-State Lett.* **7** A115 (2004)
122. M Schmid, S Kramer, C Goze, M Mehring, S Roth, P Bernier *Synth. Met.* **135-136** 727 (2003)
123. I Yu, J Lee, S G Lee *Physica B* **329-333** 421 (2003)
124. G Majer, E Stanik, S Orimo *J. Alloys Compd.* **356-357** 617 (2003)
125. K Shen, T Pietra *Appl. Phys. Lett.* **84** 1567 (2004)
126. D G Narehood, J V Pearce, P C Eklund, P E Sokol, R E Lechner, J Pieper, J R D Copley, J C Cook *Phys. Rev. B* **67** 205 409 (2003)
127. D G Narehood, M K Kostov, P C Eklund, M W Cole, P E Sokol *Phys. Rev. B* **65** 233 401 (2002)
128. Y Ren, D L Price *Appl. Phys. Lett.* **79** 3684 (2001)
129. C M Brown, T Yildirim, D A Neumann, M J Heben, T F Gennet, A C Dillon, J L Alleman, J E Fischer *Chem. Phys. Lett.* **329** 311 (2000)
130. S Challet, R Azais, R J-M Pellenq, L Duclaux *Chem. Phys. Lett.* **377** 544 (2003)
131. P A Georgiev, D K Ross, A De Monte, U Montaretto-Marullo, R A H Edwards, A J Ramirez-Cuesta, D Colognesi *J. Phys.: Condens. Matter* **16** L73 (2004)
132. A Burian, J C Dore, H E Fischer, J Sloan *Phys. Rev. B* **59** 1665 (1999)
133. K Itoh, Y Miyahara, S-i Orimo, H Fujii, T Kamiyama, T Fukunaga *J. Alloys Compd.* **356-357** 608 (2003)
134. V P Glazkov, V P Zhukov, V N Ivanova, V A Somenkov, S Sh Shil'shtein *Poverkhnost'* (6) 52 (2001)
135. H G Schimmel, G J Kearley, M G Nijkamp, C T Visser, K P de Jong, F M Mulder *Chem.-Eur. J.* **9** 4764 (2003)
136. K Shen, D L Tierney, T Pietra *Phys. Rev. B* **68** 165 418 (2003)
137. H-B Zhang, G-D Lin, Z-H Zhou, X Dong, T Chen *Carbon* **40** 2429 (2002)

138. G E Froundakis *J. Phys.: Condens. Matter* **14** R453 (2002)
139. A S Fedorov, S G Ovchinnikov *Fiz. Tv. Tela* **46** 563 (2004) [c]
140. D Levesque, A Gicquel, F Lamari Darkrim, S Beyaz Kayiran *J. Phys.: Condens. Matter* **14** 9285 (2002)
141. Q Wang, J K Johnson *J. Chem. Phys.* **110** 577 (1999)
142. X Zhang, D Cao, J Chen *J. Phys. Chem. B* **107** 4942 (2003)
143. M Volpe, F Cleri *Chem. Phys. Lett.* **371** 476 (2003)
144. F Darkrim, D Levesque *J. Phys. Chem. B* **104** 6773 (2000)
145. Y F Yin, T Mays, M McEnaney *Langmuir* **16** 10 521 (2000)
146. C W Bauschlicher Jr, Ch R So *Nano Lett.* **2** 337 (2002)
147. S M Lee, Yo H Lee *Appl. Phys. Lett.* **76** 2877 (2000)
148. Y C Ma, Y Xia, M Zhao, M Ying *Chem. Phys. Lett.* **357** 97 (2002)
149. Y C Ma, Y U Xia, M W Zhao, R Wang, L Mei *Phys. Rev. B* **63** 115 422 (2001)
150. Y Ma, Y Xia, M Zhao, M Ying *Phys. Rev. B* **65** 155430 (2002)
151. J Li, T Furuta, H Goto, T Ohashi, Y Fujiwara, S Yip *J. Chem. Phys.* **119** 2376 (2003)
152. Q Y Wang, J K Johnson *J. Phys. Chem. B* **103** 277 (1999)
153. K A Williams, P C Eklund *Chem. Phys. Lett.* **320** 352 (2000)
154. V Meregalli, M Parrinello *Appl. Phys. A* **72** 143 (2001)
155. T Yildrim, A B Harris *Phys. Rev. B* **67** 245 413 (2003)
156. J Zhao, A Buldum, J Han, J P Li *Nanotechnology* **13** 195 (2002)
157. Y Akai, S Saito *Jpn. J. Phys.* **42** 640 (2003)
158. M K Kostov, H Cheng, A C Cooper, G P Pez *Phys. Rev. Lett.* **89** 146105 (2002)
159. M M Cabli, F Toigo, M W Cole *Phys. Rev. Lett.* **86** 5062 (2001)
160. M M Cabli, F Toigo, M W Cole *J. Low Temp. Phys.* **126** 179 (2002)
161. M C Gordilio, J Boronat, J Casulleras *Phys. Rev. B* **68** 125 421 (2003)
162. M-J Ying, Y-Y Xia, M-W Zhao, X-D Liu, F Li, B-D Huang, Z-Y Tan *Chin. Phys. Lett.* **20** 550 (2003)
163. F H Yang, R T Yang *Carbon* **40** 437 (2002)
164. P-H Hou, S-T Xu, Z Ying, Q-H Yang, C Liu, H-M Cheng *Carbon* **41** 2471 (2003)
165. S M Lee, K H An, W S Kim, Y H Lee, Y S Park, G Seifert, T Frauenheim *Synth. Met.* **121** 1189 (2001)
166. C W Bauschlicher *Nano Lett.* **1** 223 (2001)
167. T Yildirim, O Gulseren, S Ciraci *Phys. Rev. B* **64** 075 404 (2001)
168. P Ruffieux, O Groning, M Bielmann, P Mauron, L Schlabach, P Groning *Phys. Rev. B* **66** 245 416 (2002)
169. D Stojkovic, P Zhang, P E Lammert, V H Crespi *Phys. Rev. B* **68** 195 406 (2003)
170. S-P Chan, G Chen, X G Gong, Z-F Liu *Phys. Rev. Lett.* **87** 205 502 (2001)
171. Y C Ma, Y Xia, M Zhao, M Ying X Liu, P Liu *Phys. Lett. A* **288** 207 (2001)
172. Y Xia, M Zhao, Y C Ma, X Liu, M Ying, L Mei *Phys. Rev. B* **67** 115 117 (2003)
173. Y Y Xia, M W Zhao, Y C Ma, M J Ying, X D Liu, P J Liu, L Mei *Phys. Rev. B* **65** 155 415 (2002)
174. S M Lee, K H An, Y N Lee, G Seifert, T Frauencheim *J. Am. Chem. Soc.* **123** 5059 (2001)
175. M Volpe, F Cleri *Surf. Sci.* **544** 24 (2003)
176. K Tada, S Furuya, K Watanabe *Phys. Rev. B* **63** 155 405 (2001)
177. Yu S Nechaev *Usp. Fiz. Nauk* **171** 1251 (2001) [*Physics-Uspekhi* **44** 1189 (2001)]
178. Yu S Nechaev *Izv. Akad. Nauk, Ser. Fiz.* **65** 1507 (2001)
179. L A Andreev, Yu S Nechaev, E A Kalashnikova, N T Konovalov, V A Lykhin, Yu A Minaev, N A Olshevskii *Phys. Status Solidi B* **163** 221 (1991)
180. Yu S Nechaev, A V Omel'chenko *Zh. Fiz. Khim.* **69** 1765 (1995) [d]
181. H Atsumi, S Tokura, M Miyake *J. Nucl. Mater.* **155-157** 241 (1988)
182. H Atsumi, K Tauchi *J. Alloys Compd.* **356-357** 705 (2003)
183. H P van Leeuwen, in *Hydrogen Degradation of Ferrous Alloys* (Eds A Oriani, J P Hirth, M Smialowski) (Park Ridges, NJ: Noyes Publ., 1985) p. 16
184. V A Bakaev, Doctoral Thesis in Physical Mathematical Sciences, Moscow State University, Moscow, 1989
185. Yu S Nechaev *Defect Diffus. Forum* **194-199** 1713 (2001)
186. V I Kostikov, Yu S Nechaev, G Ya Kul'ga *Zh. Fiz. Khim.* **76** 1583 (2002) [d]
187. Yu S Nechaev, in *Hydrogen Materials Science and Chemistry of Metal Hydrides* (Ed. N Veziroglu) (Dordrecht: Kluwer Academic, 2002) p. 161
188. M Saeki *J. Nucl. Mater.* **131** 32 (1985)
189. H Atsumi, M Iseki *J. Nucl. Mater.* **283-287** 1053 (2000)
190. J Klatte, W Ruth, W Ebenhlh *Scr. Met.* **15** 591 (1981)
191. Yu S Nechaev, S A Vladimirov, N A Olshevskii *Phys. Status Solidi* **94** 553 (1986)
192. A I Efimov, L P Belorukova, I V Vasil'kova, V P Chechev *Svoistva Neorganicheskikh Soedinenii. Spravochnik* (Properties of Inorganic Compounds. Handbook) (Leningrad: Khimiya, 1983)
193. M Kh Karapet'yants, M L Karapet'yants *Osnovnye Termodinamicheskie Konstanty Neorganicheskikh i Organicheskikh Veshchestv* (Fundamental Thermodynamic Constants of Inorganic and Organic Substances) (Moscow: Khimiya, 1968)
194. I Barin, O Knacke *Thermochemical Properties of Inorganic Substances* (Berlin: Springer, 1973)
195. M-W Zhao, Y-Y Xia, Y-C Ma, M-J Ying, X-D Liu, L-M Mei *Chin. Phys. Lett.* **19** 1498 (2002)
196. I O Bashkin, V E Antonov, E G Ponyatovskii, in *Extended Abstracts of the VIIIth International Conference 'Hydrogen Materials Science and Chemistry of Carbon Nanostructures (ICHMS'2003)', Sudak, Ukraine, 2003* p. 796
197. A Shimizu, H Tachikawa *J. Phys. Chem. Solids* **64** 419 (2003)
198. A A Zhukhovitskii, L A Shvartsman *Fizicheskaya Khimiya* (Physical Chemistry) (Moscow: Metallurgiya, 1987)
199. I E Gabis, E A Evard, A P Voit, S K Gordeev, in *Proceedings of the VIIth International Conference 'Hydrogen Materials Science'* (Kiev: ADEF-Ukraine, 2001) p. 700
200. E A Evard, A P Voit, S K Gordeev, I E Gabis *Mater. Sci.* **36** 499 (2000)
201. E A Denisov, T N Kompaniets *Zh. Tekhn. Fiz.* **71** 111 (2001) [e]
202. P G Shewman *Diffusion in Solids* (New York, London: Wiley, 1962)
203. Yu S Nechaev, K H G Egziabher *Phys. Status Solidi A* **106** 399 (1988)
204. M Cinke, J Li, B Chen, A Cassell, L Delzeit, J Han, M Meyyappan *Chem. Phys. Lett.* **365** 69 (2002)
205. US P. 5 653 951 (1997)
206. A Chambers, T Nemes, N M Rodriguez, T K Baker *J. Phys. Chem. B* **102** 2251 (1998)

[a] — *Physics-Uspekhi (Engl. Transl.)*
[b] — *J. Exp. Theor. Phys. Lett. (Engl. Transl.)*
[c] — *Phys. Solid State (Engl. Transl.)*
[d] — *Russ. J. Phys. Chem. (Engl. Transl.)*
[e] — *J. Techn. Phys. (Engl. Transl.)*